ARL-TR-8931 ● APR 2020

DEVCOM ARMY RESEARCH LABORATORY

Implementation and Evaluation of the World's Largest Outdoor Optical Motion-Capture System

by Daniel Everson and Barry Kline

NOTICES

Disclaimers

The findings in this report are not to be construed as an official Department of the Army position unless so designated by other authorized documents.

Citation of manufacturer's or trade names does not constitute an official endorsement or approval of the use thereof.

Destroy this report when it is no longer needed. Do not return it to the originator.

ARL-TR-8931 ● APR 2020

Implementation and Evaluation of the World's Largest Outdoor Optical Motion-Capture System

Daniel Everson
Weapons and Materials Research Directorate, CCDC Army Research Laboratory

Barry Kline
SURVICE Engineering

REPORT DOCUMENTATION PAGE

Form Approved
OMB No. 0704-0188

1. REPORT DATE *(DD-MM-YYYY)*	2. REPORT TYPE	3. DATES COVERED (From - To)
April 2020	Technical Report	May 2017–October 2019

4. TITLE AND SUBTITLE
Implementation and Evaluation of the World's Largest Outdoor Optical Motion-Capture System

5a. CONTRACT NUMBER

5b. GRANT NUMBER

5c. PROGRAM ELEMENT NUMBER

6. AUTHOR(S)
Daniel Everson and Barry Kline

5d. PROJECT NUMBER

5e. TASK NUMBER

5f. WORK UNIT NUMBER

7. PERFORMING ORGANIZATION NAME(S) AND ADDRESS(ES)
CCDC Army Research Laboratory
ATTN: FCDD-RLW-LF
Aberdeen Proving Ground, MD 21005

8. PERFORMING ORGANIZATION REPORT NUMBER
ARL-TR-8931

9. SPONSORING/MONITORING AGENCY NAME(S) AND ADDRESS(ES)

10. SPONSOR/MONITOR'S ACRONYM(S)

11. SPONSOR/MONITOR'S REPORT NUMBER(S)

12. DISTRIBUTION/AVAILABILITY STATEMENT
Approved for public release; distribution is unlimited.

13. SUPPLEMENTARY NOTES
ORCID ID: Daniel Everson, 0000-0003-0466-1132

14. ABSTRACT
The US Army Combat Capabilities Development Command Army Research Laboratory Guidance Technologies Branch has implemented a one-of-a-kind outdoor motion-capture system for multi-agent unmanned aerial system testing. This system consists of 96 cameras housed within 16 tracking pods positioned around the perimeter of the desired capture volume. The cameras track actively illuminated LED marker strobes attached to test articles moving throughout the volume. Recent evaluation of this system demonstrated accurate marker tracking within a 460- × 110- × 70-m volume at a measurement rate of 100 Hz.

15. SUBJECT TERMS
outdoor motion capture, multi-agent tracking, swarming, unmanned aerial system (UAS) operations, navigation ground truth

16. SECURITY CLASSIFICATION OF:			17. LIMITATION OF ABSTRACT	18. NUMBER OF PAGES	19a. NAME OF RESPONSIBLE PERSON
a. REPORT	b. ABSTRACT	c. THIS PAGE			Daniel Everson
Unclassified	Unclassified	Unclassified	SAR	65	19b. TELEPHONE NUMBER (Include area code) (410) 278-4693

Standard Form 298 (Rev. 8/98)
Prescribed by ANSI Std. Z39.18

Contents

List of Figures

List of Tables

1. Introduction

The US Army Combat Capabilities Development Command Army Research Laboratory (ARL) is actively pursuing technologies under the Precision and Cooperative Weapons in a Denied Environment (PCWDE) mission program to perform navigation in GPS-denied and -degraded conditions.[1,2] The objective of guided lethality research is to provide assured delivery of a projectile payload to increase performance and widen the engagement space. Several of the key research areas, including vision-based navigation and swarming behavior, attempt to solve technical challenges associated with operating in degraded or compromised environments. To achieve research goals, researchers must be able to validate navigation and swarming technical solutions.

To meet the PCWDE objectives, a unique experimental research capability has been established. This large-scale, outdoor motion-tracking system will provide researchers with the ability to precisely localize agents of an aerial swarm. Small and medium-size unmanned aerial vehicles equipped with navigation devices will serve as development platforms for vision-based navigation solutions and swarming-guidance strategies. The ability to deliver precision tracking of large-scale, multi-agent experiments in an outdoor environment will enable research that could not be accomplished with previously existing facilities at ARL or elsewhere.

2. Background

Motion-capture at a fundamental level is the process of recording the movement of objects through space. Modern motion-capture systems expand on this concept to simultaneously track multiple objects or multiple points on a single object at high precision and high measurement rates. Tracking multiple points on a rigid body enables a motion-capture system to estimate the attitude of the object in addition to its position as a function of time. Tracking multiple points on an articulated body such as a robot or a human actor enables the mapping of motion-capture data to a kinematic model of the articulated body.

Motion-capture systems are commonly used by the entertainment industry to generate animated elements of cinematography based off of the motion of human actors.[3] Academic researchers developing complex robotic devices leverage motion-capture systems to provide near-real-time estimation of the state of the devices with respect to their environment. This technique enables the implementation of control techniques requiring feedback that exceeds the capability of onboard sensors.[4] Simultaneous tracking of multiple independent robotic devices also allows researchers to investigate swarming concepts.[5–7]

Motion-capture systems are well suited to provide a ground-truthing capability for researchers developing navigation sensors for autonomous systems. By independently recording the motion of a test vehicle at high spatial and temporal resolutions, a motion-capture system can provide valuable data for evaluation of sensor data recorded onboard the test vehicle.[8]

There are a variety of fundamental technologies used by different motion-capture systems to estimate the position of objects as a function of time. These include systems based on inertial measurement units, sensing of magnetic fields, and radio ranging devices.[9] However, the majority of motion-capture systems employed by the entertainment industry and academia use optical sensors and stereo-vision techniques to produce position estimates for special optical markers at the frame rate of the vision sensors.

Optical motion-capture systems must rapidly and reliably detect markers as they move within a designated capture volume. This requires the markers to be easily distinguishable from the visible background. This is typically achieved by imaging the markers in a specific wavelength and relying on optical filters to increase the relative sensitivity of the optical sensors in that specific wavelength. Markers used with optical motion-capture systems are typically either passive or active based on the application and a series of advantages and disadvantages for each type. Passive markers reflect light generated by a strobe that emits light in a wavelength consistent with the design of the optical sensor. Active markers directly emit light in the appropriate wavelength.

In 2016 ARL identified an emerging need for an experimental capability that did not then exist. Evaluation of technologies developed under the PCWDE mission research program will require experiments consisting of multiple simultaneously operating unmanned aerial systems (UASs) acting as projectile surrogates.[10–13] Additional experiments will use soft-launched projectiles outfitted with candidate electronics components. These experiments will require accurate ground truth measurements of agent position collected at a data rate and level of precision that exceeds the capability of current GPS technologies. The measurement attributes of motion-capture systems make those technologies attractive options to meet this need, but no existing system was capable of meeting ARL's requirements. Implementation of a motion-capture system to service a large outdoor range space presents inherent challenges that no existing technology was capable of achieving.

2.1 Motion-Capture Technology Survey

ARL conducted a detailed technology survey to identify candidate technologies with potential to meet the experimental needs of the PCWDE research effort. The majority of possible options were either technically immature or could not be scaled to the size of the capture volume required by ARL. The one approach that was found to be feasible was optical motion-capture. Several vendors had demonstrated implantation of their optical motion-capture systems in outdoor environments. Specifically, outdoor motion-capture using actively illuminated markers was found to be the most viable strategy. The use of high-power active markers, properly implemented, generates enough signal above the noise of ambient solar radiation to allow for optical detection at distances sufficient for instrumentation of a large capture volume.

2.2 Motion-Capture System Performance Requirements

ARL established a set of requirements for an outdoor motion-capture system to support the needs of the PCWDE research effort. Required functional performance parameters are shown in Table 1.

Table 1 Motion-capture system performance requirements established by ARL

Requirement	Objective	Threshold
Provides near-real-time tracking results	Yes	Yes
System coverage area length/width/height (m)	500/200/200	300/60/75
Marker integration volume (cm^3)	63	270
Maximum agent velocity (m/s)	100	50
Number of agents	100	10
Position accuracy (m)	0.01	0.5
Measurement of vehicle attitude (6 degrees of freedom [DOF])	Yes	No
Measurement update rate (Hz)	100	10

In addition to these performance characteristics, a series of additional design considerations was developed to inform development of a capability suitable for ARL's specific needs. These considerations included the following:

- Tracking reliability of markers in ambient daylight conditions
- Disambiguation of markers located on multiple agents operating in close proximity

- Integration of markers into projectile flight hardware. Sample case provided was an 83- ×50-mm-tall "puck" section of a cylindrical projectile
- Setup/breakdown time for the system. Intended use is temporary instrumentation of a shared use range facility for test events of 1 week's duration
- Consideration of environmental conditions and associated weatherproofing to support year-round testing at Aberdeen Proving Ground, Maryland

2.3 Contracting for System Development

Because the survey of existing technologies indicated that a system to meet these requirements did not exist, a two-phase contracting approach was used to pursue a solution. The intent of the first phase was to fund multiple vendors to demonstrate their existing technologies and develop a proposal to extend the capability of those technologies to meet the full-system requirements. The results of the first phase would then be used to select a single vendor to deliver on their proposed solution in a second phase.

In May 2017, ARL awarded a Phase 1 contract to PhaseSpace, Inc., as the only vendor who submitted a viable response to the ARL request for proposals. At the conclusion of the first phase, ARL subject matter experts determined that the proposed full solution presented by PhaseSpace was viable given the maturity level of their demonstrated existing technology. In August 2017, ARL awarded a second phase contract for development, implementation, and demonstration of the proposed system.

3. Large Outdoor Motion-Capture Technical Solution

The outdoor motion-capture system developed by PhaseSpace to meet ARL's requirements consists of 16 individual tracking pods housing six cameras each, a total of 96 cameras. Each camera consists of a 5-megapixel vision sensor outfitted with a 21-mm prime lens, providing a horizontal field of view (FOV) of approximately 33°. The six cameras within each pod are arranged in two rows of three, with the cameras oriented such that the FOV of each slightly overlaps the adjacent cameras. This arrangement provides a total FOV for each pod of approximately 100° horizontal by 42° vertical. Spacing 16 pods around the perimeter of a desired capture volume with inward-facing, overlapping FOVs enables 3-D position tracking of actively illuminated markers using stereo-vision techniques.

3.1 Tracking Pod Design

Sixteen individual tracking pods serve as the primary component of the outdoor motion-capture system. These pods allow a team tasked with setting up the system to quickly place an array of six cameras and the associated support hardware at an appropriate location as a single unit. The pods also serve as a weathertight enclosure for the cameras, allowing the units to be left in place over the duration of a multiple-day test event.

Each pod consists of an aluminum platform that mounts to a pod stand approximately 36 inches tall. Adjustable feet on the base of the pod stand allow the pod to be leveled as necessary to accommodate uneven ground. An internal aluminum frame structure provides mounting surfaces for the electronics components that make up the functional elements of each pod. Six custom-designed cameras with purpose-built flanged housings rigidly affix to the internal frame in a configuration that provides adjoining FOVs with a small amount of overlap. The configuration of cameras and other internal components is shown in Fig. 1. Two motherboards control the cameras and process image frames for detection of markers. A network switch enables connectivity between each pod and a central server through a system of daisy-chaining multiple pods together. Thermal management of the internal electronics is provided by a series of fans and a large heat-sink located on the rear exterior of the pod. An aluminum outer case provides a weathertight enclosure to protect the internal electronics from the ambient environment, as shown in Fig. 2. A GPS receiver is located in a separate exterior enclosure affixed to the top of the pod with a data feed into the pod to provide timing data necessary for synchronization of cameras and markers.

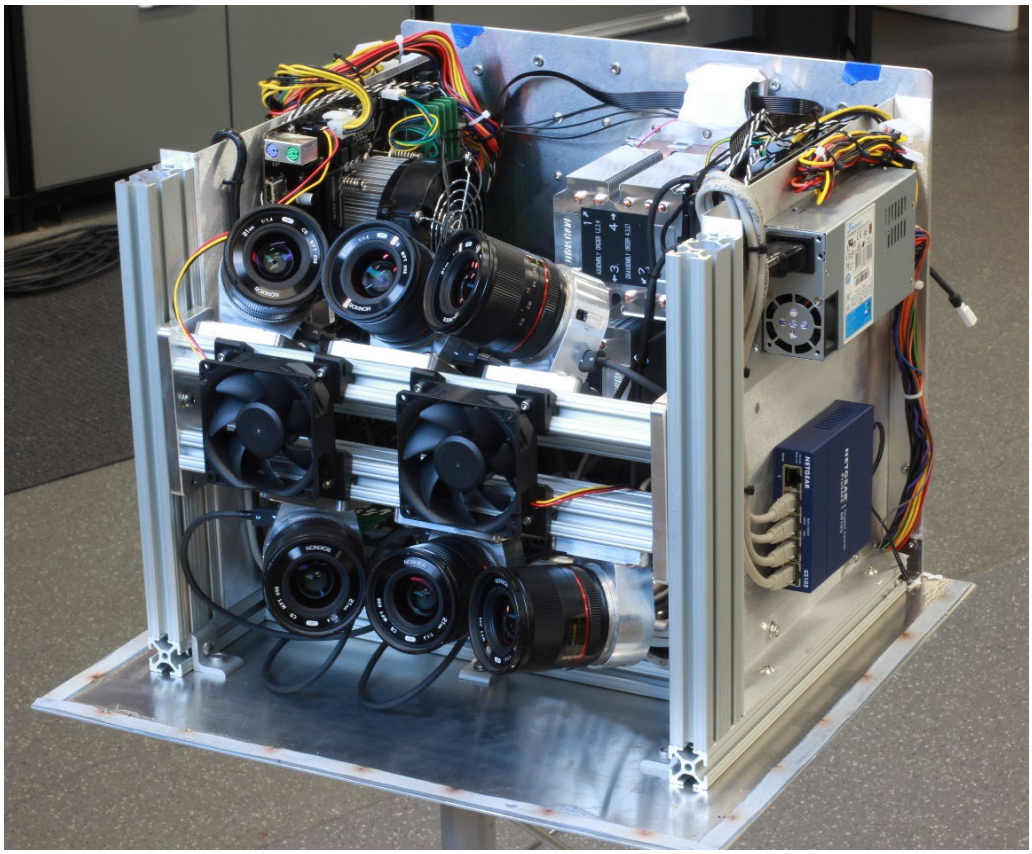

Fig. 1 Internal components of a tracking pod including six cameras with overlapping FOVs

Fig. 2 Complete tracking pod atop aluminum pod stand

3.2 Active LED Marker Design

Actively emitting LED markers provide a bright light source that is readily detectible by the tracking pods at extended ranges in normal daylight conditions. A marker configuration was developed by PhaseSpace to meet ARL's requirement for marker implementation in a projectile form factor. This configuration is also suitable for implementation on UASs. The marker consists of an 83-mm-diameter printed circuit board (PCB) with 96 surface-mounted LEDs located around the annulus of the PCB, as shown in Fig. 3. A quarter-radius aluminum reflector mounted above the LEDs results in good visibility of emitted light from locations parallel to the plane of the PCB approximately ±40°. A GPS receiver located on a second, companion PCB provides a timing signal that allows the marker strobe to synchronize the LEDs with cameras in the tracking pods. The markers achieve an extremely bright output to enable detection by the cameras by strobing the 96 LEDs at 3 W each in sync with frame exposures on the cameras. Although the instantaneous power consumption of the marker is high, the duty cycle is very short, which keeps overall power consumption at an acceptable level.

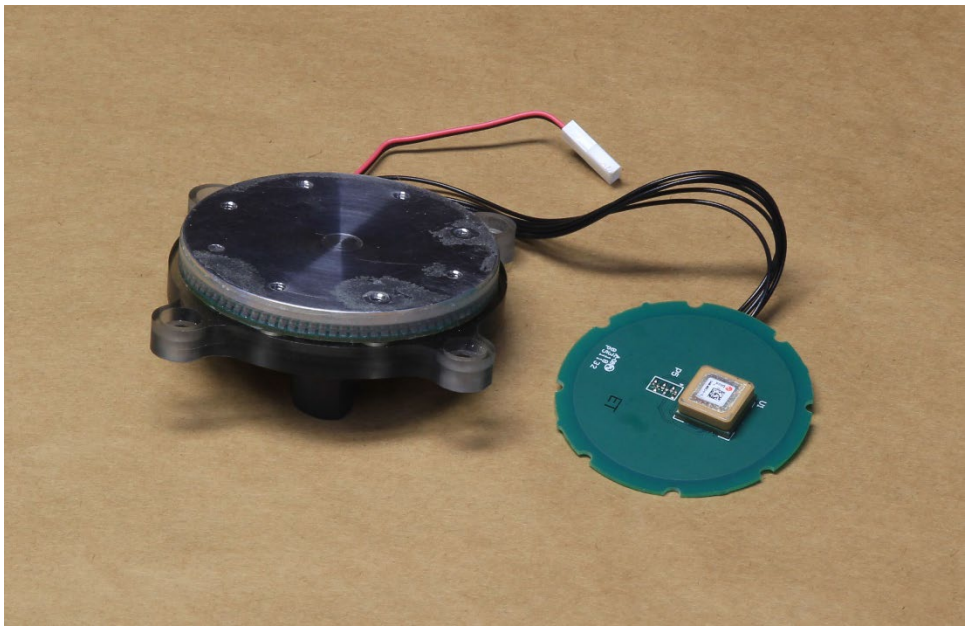

Fig. 3 Active marker strobe consisting of 96 LEDs located around the perimeter of a custom PCB. A second PCB with a GPS receiver provides timing for synchronization with cameras.

PhaseSpace has implemented a patented[14] method that allows disambiguation of multiple markers being simultaneously tracked by the system. Each marker broadcasts a unique code by modulating the output intensity of its LEDs on successive frames. Detection and interpretation of this modulation allows unique identification of markers to be established from a sequence of frames.

3.3 Marker Detection

The primary technical barrier to implementation of an outdoor motion-capture system of the proposed scale is the detection of markers at extended range in ambient outdoor lighting conditions. Radiant energy available to a sensor decreases as a function of distance from the source according to the inverse square law.[15] As the distance between the active markers and the tracking pods increases, the relative intensity of the marker with respect to ambient solar radiation decreases. When this signal-to-noise ratio reaches a critically low level, the marker can no longer be reliably detected. PhaseSpace has addressed this challenge by optimizing the camera configuration to increase relative sensitivity to the output of the active markers while decreasing sensitivity to solar radiation. This is achieved by using optical notch filters tuned to the emission wavelength of the active markers. The cameras also implement a global shutter synchronized with the output pulses of the active markers. Minimization of the sensor integration time while maintaining an adequate exposure interval to capture the entire pulse of the LED marker increases

the signal-to-noise ratio. Because the output pulses from the active markers are very short in duration to maximize the marker intensity while controlling the overall duty cycle of the LEDs, the markers and cameras need to be synchronized to within a few microseconds. Timing output from GPS receivers on both the active markers and the tracking pods allows for this level of synchronization even though the devices are operating remotely.

3.4 System Configuration

Wired connections between tracking pods are required to provide both power and a data path between the pods and a central tracking server. A pair of 7000-W inverter generators are used to provide power to the system in range environments where line power is not readily available. Each tracking pod has external connectors for input and output AC power, allowing power for multiple pods to be daisy-chained between pod locations using a series of 75-m-long power cables. Similarly, a pair of external Ethernet ports are available on each pod. These ports, in conjunction with the internal network switch present within each pod, allow a daisy-chain data network in which each pod is connected to neighboring pods via 75-m-long Category 6 Ethernet cables. The pods closest to the central tracking server are connected to the server directly, providing connectivity between all 16 pods and the tracking server.

Each tracking pod is capable of detecting and classifying the light output by active markers present within the FOV of the pod's six cameras. These data are transmitted via the Ethernet network to the tracking server, which processes this information using calibrated models of the cameras, pods, and system layout, to perform a stereo-vision optimization and estimate the positions of the markers within the capture volume.

3.5 System Implementation for Collection of Motion-Capture Data

Implementation of the motion-capture system for a given test event starts with pretest planning of the system layout based on the test objectives and the physical constraints of the range environment. ARL developed a model of the camera FOV for each tracking pod in MATLAB. A depiction of the FOVs of all six cameras associated with a single tracking pod is shown in Fig. 4. This model is used to visualize the camera FOVs for multiple pods in a proposed system layout. The overlapping FOV from the array of tracking pods is assessed to verify that adequate camera coverage in combination with orthogonal perspectives between pods is

available to support the test objectives. A notional system layout for a range space with a footprint of 465 × 110 m is shown in Fig. 5.

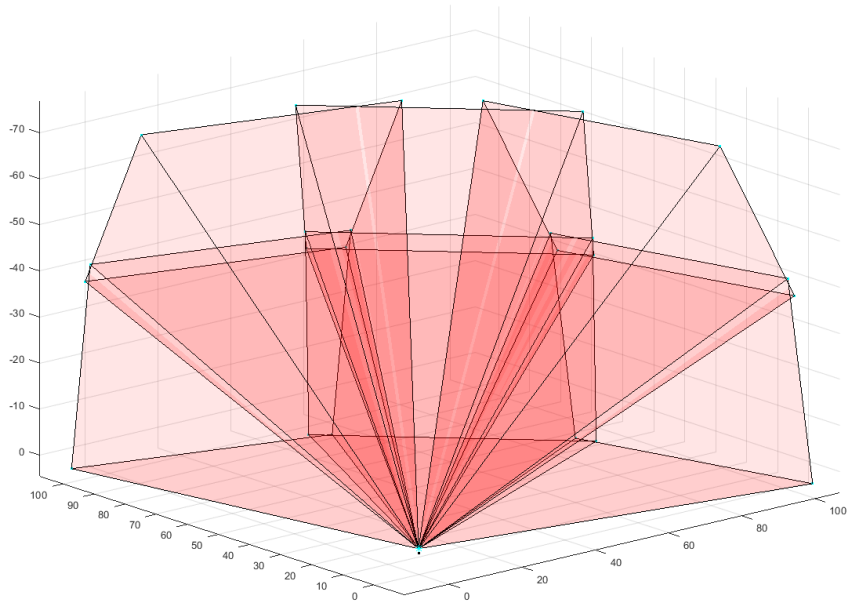

Fig. 4 Model of camera FOVs for the six cameras within each tracking pod

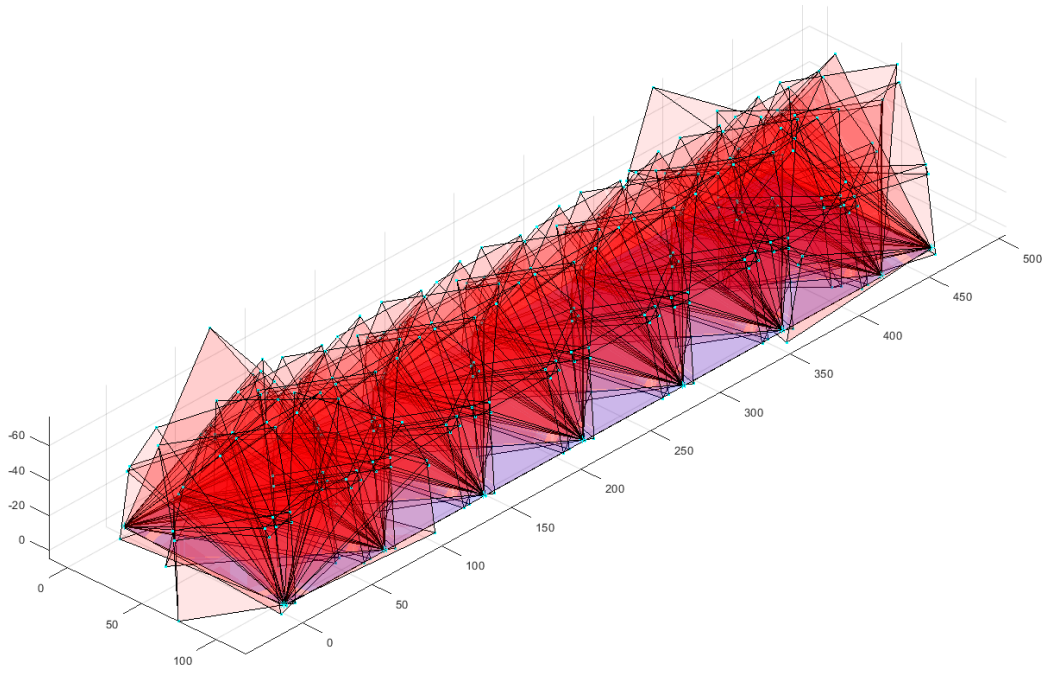

Fig. 5 Camera FOV for all tracking pods in a notional 465- × 110-m system layout

Survey equipment is used to stake out the planned location of the tracking pods at the selected test range. ARL uses a Leica TS16 total station for this task. This instrument is not only effective for laying out the system configuration, but is also

used to accurately measure the position of the pods in a local coordinate system once they have been set up. ARL has outfitted a box trailer for storage and transportation of the tracking system hardware and associated equipment. If feasible, this trailer is used to haul the tracking pods directly to each planned location. Physical setup of each tracking pod consists of the following basic steps:

- Place the pod stand at the planned location
- Attach the pod to the stand
- Orient the pod according to the planned layout
- Level the pod using the adjustable feet on the pod stand
- Unspool Ethernet and power cables and connect to adjacent pods as appropriate

Prior to powering up the system and performing pretest calibration, the location of each tracking pod must be measured in the local coordinate system that will be used throughout the test event. This task is accomplished by using the TS16 and a Leica 360° mini-prism placed on a reference mark on the top of each pod. The pod locations are a required input into the system-calibration routine and allow the system to be oriented to the local coordinate system for the collection of motion-capture data in that frame.

Calibration of the system requires collection of a multitude of frames in which a common marker is visible from multiple cameras. The calibration data set should preferably include instances when the marker is located throughout the planned capture volume and spanning the FOV of each camera. These data are then fed into an optimization routine that estimates the pose of each tracking pod and its associated cameras. For typical motion-capture systems, this task is accomplished by manually moving a calibration wand outfitted with multiple markers throughout the desired capture volume. However, due to the large outdoor capture volume, this approach is not viable. To efficiently move a marker throughout the capture volume, a UAS is outfitted with a marker and flown in a pattern designed to cover as much of the capture volume as is practical.

Once adequate calibration data has been collected, the tracking server processes these data in conjunction with the surveyed location of each tracking pod to produce a calibration solution. The calibration solution consists of the pose of each of the 96 cameras comprising the motion-capture system in addition to a model of the camera intrinsics for each camera. This information is used by the system to estimate the position of detected markers in near-real time once the test event begins.

4. Performance Evaluation Test Event

A test event was conducted at Aberdeen Proving Ground, Maryland, during August 2019 to demonstrate the functionality of the outdoor motion-capture system and to characterize the system performance. The range location selected for this test event consisted of an open field approximately 120 × 700 m bordered by a perimeter gravel road. This site is typically used by ARL for conducting navigation research experiments with UASs acting as surrogates for tactical systems. It is expected that future test events leveraging the capability of the outdoor motion-capture system will also use this site, making it a suitable location for evaluation of system performance.

Pretest planning generated a system configuration for two parallel rows of eight tracking pods each, with pods paced at the edge of the open field. The system layout overlaid on satellite imagery of the selected test range is shown in Fig. 6. This configuration provides an effective capture volume of approximately 465 m long by 110 m wide by 60 m tall.

Setup of the motion-capture system using the process described in Section 3.5 required a team of four personnel and 4.5 h of continuous effort to transition from arrival of equipment on site in the box trailer to fully set up and ready the system-calibration sequence. The planned location of all equipment had been surveyed and marked by paint on a previous day.

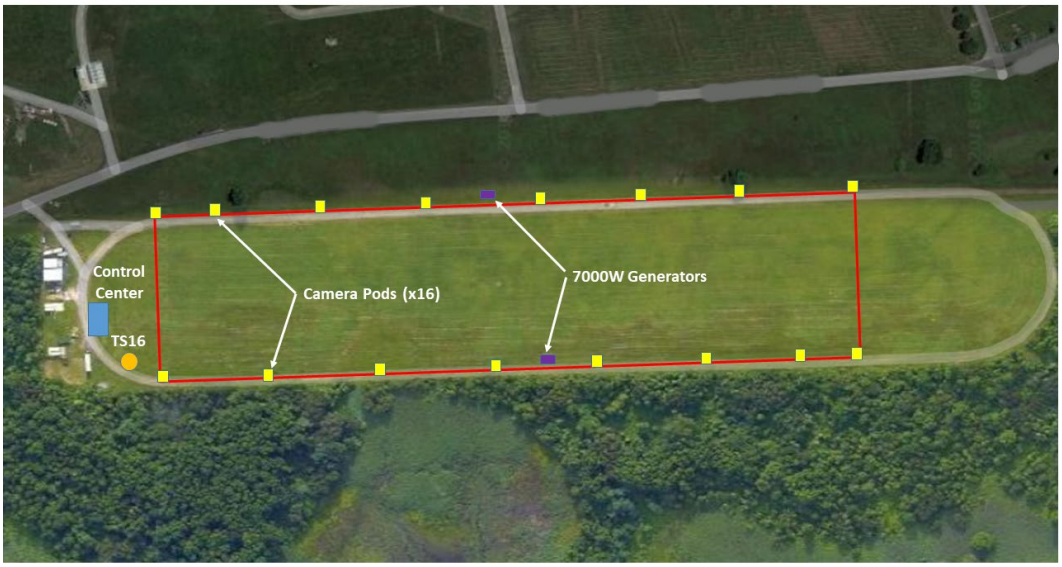

Fig. 6 Planned system layout for evaluation of motion-capture system performance

4.1 System Calibration

Calibration data were collected using ARL's GRB R600 UAS outfitted with an active marker mounted on the underside of its reconfigurable payload platform, as shown in Fig. 7. Prior evaluation efforts conducted during system development identified a multi-tiered "lawnmower" pattern as an effective flight path to generate adequate calibration data by moving the calibration marker throughout all regions of the capture volume. The UAS flight plan for collection of system calibration data for this test event is shown in Fig. 8. This UAS flight lasts approximately 23 min, resulting in more than 130,000 frames of marker position to feed into the calibration-optimization routine. Processing this calibration requires approximately 20 additional min of computer processing time on the tracking server located in the control center. Once a calibration solution is achieved, the system is ready to track markers in support of the test event.

Fig. 7 GTB R600 UAS outfitted with marker strobe and 360° survey prism

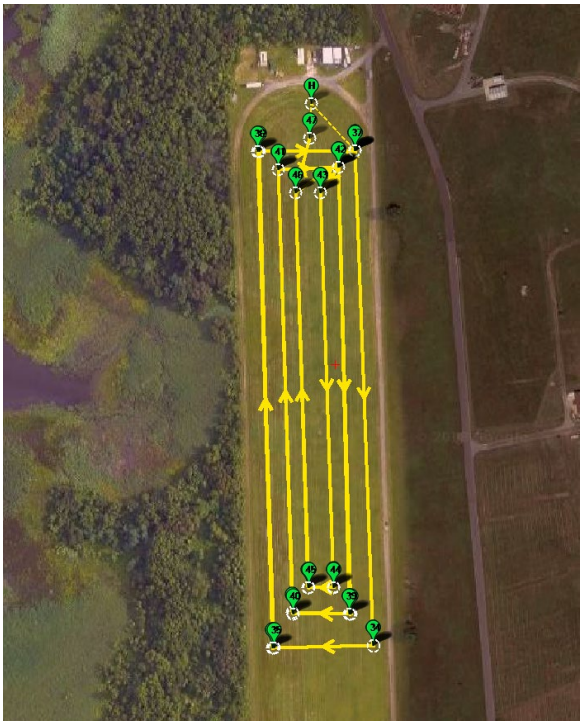

Fig. 8 UAS flight plan for collection of system-calibration data

4.2 System Performance Evaluation Methods

ARL developed three separate approaches to evaluate the performance of the motion-capture system. A UAS outfitted with a tracking marker was simultaneously tracked by the motion-capture system, and traditional survey equipment with the traditional survey equipment provided ground-truth data to evaluate the accuracy of the motion-capture system position estimates. A rigid rotating arm was used to move a marker through a repeatable circular path of known radius to evaluate the precision of the motion-capture system position estimates. A manually launched projectile surrogate was used to demonstrate the ability to integrate an active marker into a projectile form factor and to demonstrate the ability of the system to track a marker at higher velocities than could be achieved with the other devices.

4.3 Collection of Data for Evaluation of Tracking Accuracy

The same GTB R600 UAS was used to generate position measurements for evaluation of the motion-capture system tracking accuracy. The UAS was flown on a flight path consisting of five concentric circles of decreasing diameter in the horizontal plane, with that pattern repeated at six altitude levels. This flight path was designed to allow the UAS to efficiently generate position data throughout a large portion of the capture volume, resulting in an effective data set for evaluation

of the motion-capture system performance throughout the motion-capture volume as a whole.

The GTB R600 was outfitted with a 360° reflective prism mounted just below a tracking marker, as shown in Fig. 9. ARL's TS16 robotic total station[16] is capable of autonomously tracking this reflective prism and collecting survey-grade measurements of the prism position at a measurement rate of approximately 5 Hz. Measurements collected by the TS16 are referenced to the same local coordinate system used for calibration of the motion-capture system and serve as an effective ground truth to evaluate the measurement accuracy of the motion-capture system. Note that the measurement accuracy of the TS16 is estimated by the instrument for each recorded measurement and is a function of the range between the instrument and the reflective prism. For the scale of this test, the largest 3-D measurement error bound provided by the TS16 instrument was 0.03 m. This position measurement accuracy is approximately an order of magnitude better than the required accuracy of the motion-capture system, providing adequate accuracy to serve as a ground-truth system.

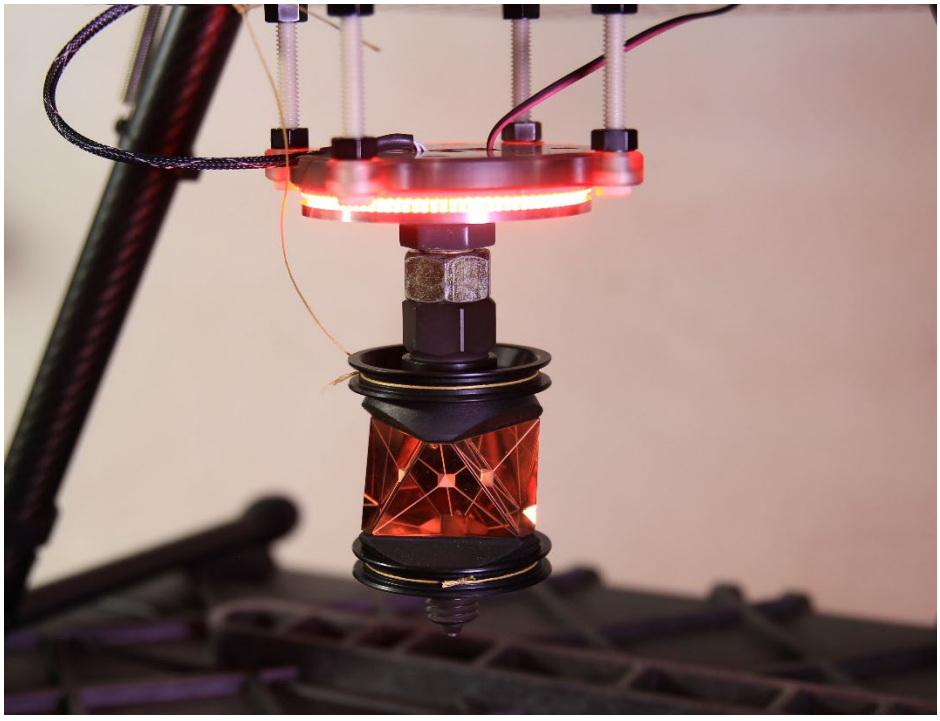

Fig. 9 360° survey prism mounted in a stacked configuration with a marker strobe for the simultaneous collection of motion-capture and ground-truth measurements

It was determined after the conclusion of the test event that the timing accuracy of the TS16 was not as accurate as anticipated, resulting in frequent timing errors of up to 0.08 s and occasional errors up to 0.3 s. Given that the UAS velocity during the data-collection flights was typically between 4 and 6 m/s, timing errors of this magnitude result in the inability to directly compare measurements produced by the motion-capture system against raw measurements from the survey instrument. Postprocessing of the TS16 measurements was required to correct timing errors, as detailed in Section 5.1. In hindsight it would have been beneficial to collect an additional series of measurements with the UAS hovering in several static locations. These measurements would allow for spot checking of measurement accuracy without a strong dependence on the timing accuracy of the TS16 measurements. However, due to the time investment required, repeating the test to collect these additional measurements was not possible.

4.4 Collection of Data for Evaluation of Tracking Precision

A rigid rotating-arm device was implemented to provide repeatable, constrained motion of a tracking marker for the generation of data suitable for the evaluation of repeatability and precision of measurements generated by the motion-capture system. This device consisted of a 10-ft aluminum bar with a marker attached to one end and a counterweight attached to the other, as shown in Fig. 10. This bar was affixed to a rotating stage mounted atop a large tripod. The result of this configuration was a device that could be manually rotated to produce repeatable circular motion of the marker with a fixed radius of rotation of 2.28 m.

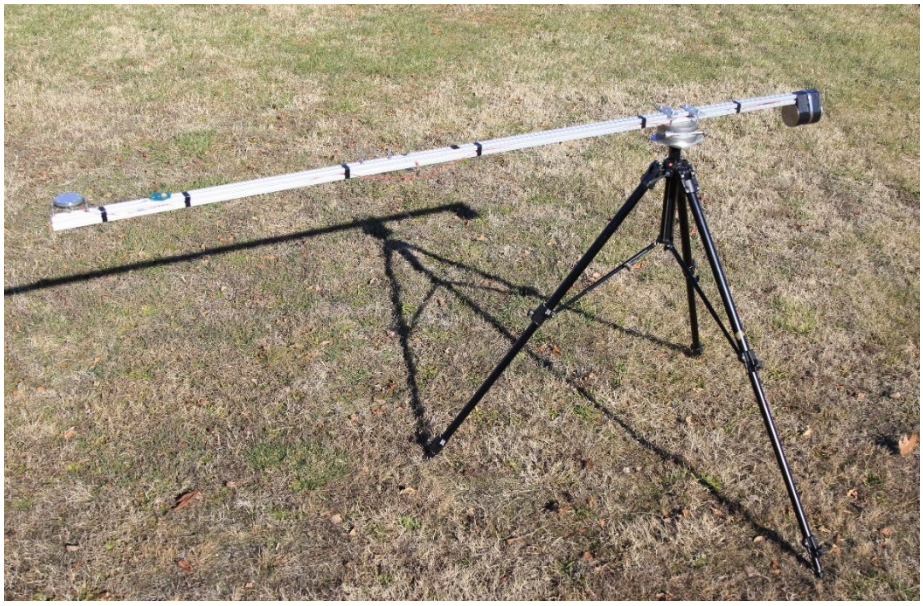

Fig. 10 Rigid rotating-arm device for collecting data to evaluate motion-capture system measurement precision

4.5 Tracking a Marker Integrated in a Projectile Form Factor

A fin-stabilized surrogate projectile was designed for integration of the 83-mm-diameter active marker developed by PhaseSpace. This projectile was fabricated from glass-filled nylon using a selective-laser-sintering additive manufacturing technique. The tracking marker was located in the middle of the projectile body, as would be conceptually feasible for an actual projectile-based test event. This projectile as configured for testing is shown in Fig. 11. It was manually launched using an 11-ft-long fishing rod by attaching a short piece of Dacron line to the aft of the projectile and casting the projectile as would be done while surf casting with a heavy weight. This method was capable of producing projectile velocities greater than 30 m/s, trajectories of up to 90 m long, and times of flight of approximately 4 s.

Fig. 11 Surrogate projectile for demonstration of marker integration in a projectile configuration and collection of position measurements for a high-speed object

5. Analysis of Collected Data to Establish Observed System Performance

Position-tracking performance of the motion-capture system was evaluated by postprocessing data in MATLAB. Data sets generated by both the motion-capture system and the TS16 were converted into ASCII text files and then imported into the MATLAB workspace for further manipulation. Specific analysis methods were used on the data sets collected as described in Sections 4.3–4.5 to evaluate measurement accuracy, measurement precision, and tracking of a projectile configuration.

5.1 Evaluation of Position-Tracking Accuracy

Measurements produced by the TS16 survey instrument serve as the ground truth for position-tracking accuracy. Ideally, these measurements would be directly compared against measurements generated by the motion-capture system as a function of time. Even though the measurements from the two systems are not synchronous, simple interpolation techniques could be used to generate a basis for comparison. However, as mentioned in Section 4.3, it was immediately obvious upon attempting this approach that the timing accuracy of the total station measurements was not adequate for the associated measurements to serve as a ground truth in their raw state. Note that a GS16 survey GPS receiver was connected to the TS16 while data were being collected in an attempt to provide a GPS timing signal and ensure timing accuracy of the TS16 measurements, but even this approach proved to be inadequate.

Leica technical support was contacted for an in-depth investigation into the way in which the TS16 timestamps its recorded measurements. Based on this information and a manual evaluation of the TS16 data, it is assumed that the position values of collected measurements are valid within the accuracy of the instrument and only the timestamps are inaccurate. Leveraging this assumption, an algorithm was created to correct the timestamps of the TS16 data. Details of this algorithm and the resulting postprocessed data used for ground-truthing are presented in the Appendix. Note that the position estimates generated by the motion-capture system were used as an input to the algorithm for correcting the TS16 measurement timestamps. Accordingly, the timestamp corrections are inherently biased to reduce the error between the motion-capture measurements and the ground truth. The postprocessing algorithm to correct the TS16 timestamp errors was designed to minimize this effect, as described in the Appendix. However, the measurement accuracy results presented in this section are likely a slight underestimate of the true measurement error.

Linear interpolation in 3-D was used on the postprocessed TS16 measurements to generate a basis for comparison against the motion-capture measurements at the native measurement rate of the motion-capture system. Linear interpolation between data points of the TS16 data assumes that the UAS was operating at constant velocity between data points. This assumption will produce negligible error when the data points are densely spaced in time. However, larger time gaps will result in intermediate data points that do not reflect the true position of the UAS. To prevent these gaps in the ground-truth data from skewing the analysis results, all time gaps greater than 0.4 s were excluded from the comparison data set. After applying this filter, the comparison data set included 98,105 data points

captured by the motion-capture system, representing more than 16 min of cumulative data collection.

Comparison of position measurements from the motion-capture system and the ground truth in each of the principal directions of the local coordinate system was used to generate orthogonal elements of position error as a function of time. The error components are calculated using Eq. 1, where p represents the true position, $\hat{p}$ represents the estimated position, e represents the position error, and the subscripts N, E, and D indicate the orthogonal components in the Northing, Easting, and Down directions, respectively. Position error along each principal axis as a function of time is shown in Fig. 12.

$$\begin{aligned} e_N &= \hat{p}_N - p_N, \\ e_E &= \hat{p}_E - p_E, \\ e_D &= \hat{p}_D - p_D. \end{aligned} \tag{1}$$

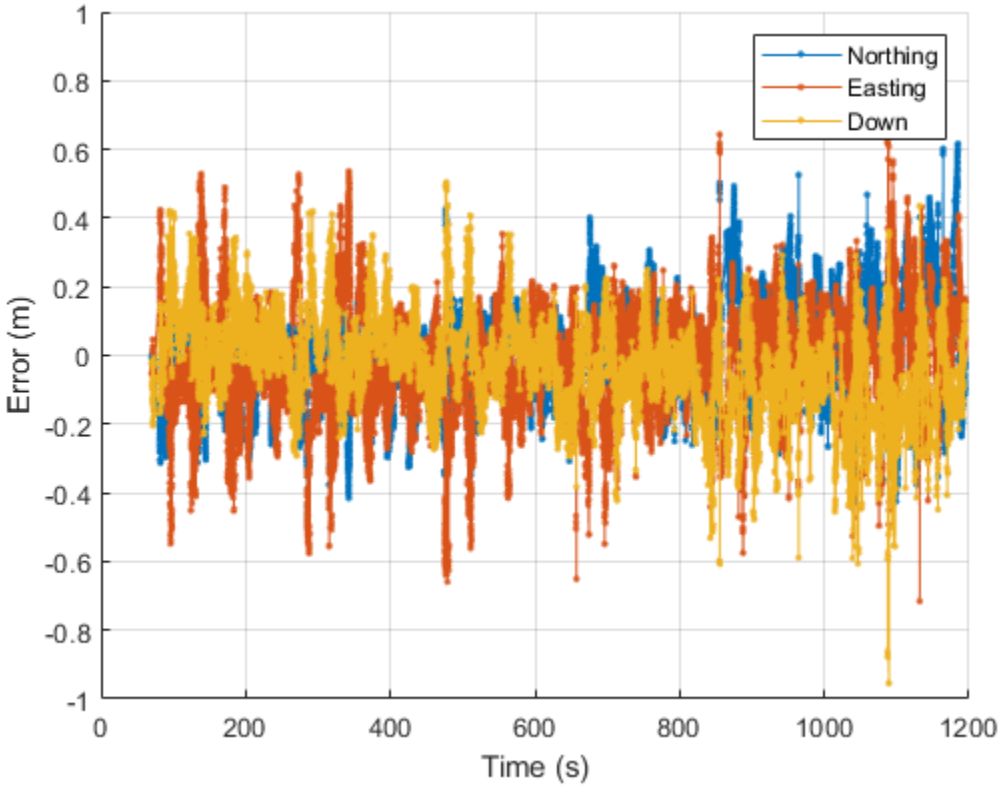

Fig. 12 Orthogonal components of position measurement error as a function of time

The three error components were combined to generate an estimate of the 3-D position-error magnitude at each sample point using Eq. 2, where the subscript T represents the total position error, shown as a function of time in Fig. 13.

$$e_T = \sqrt{e_N{}^2 + e_E{}^2 + e_D{}^2}. \quad (2)$$

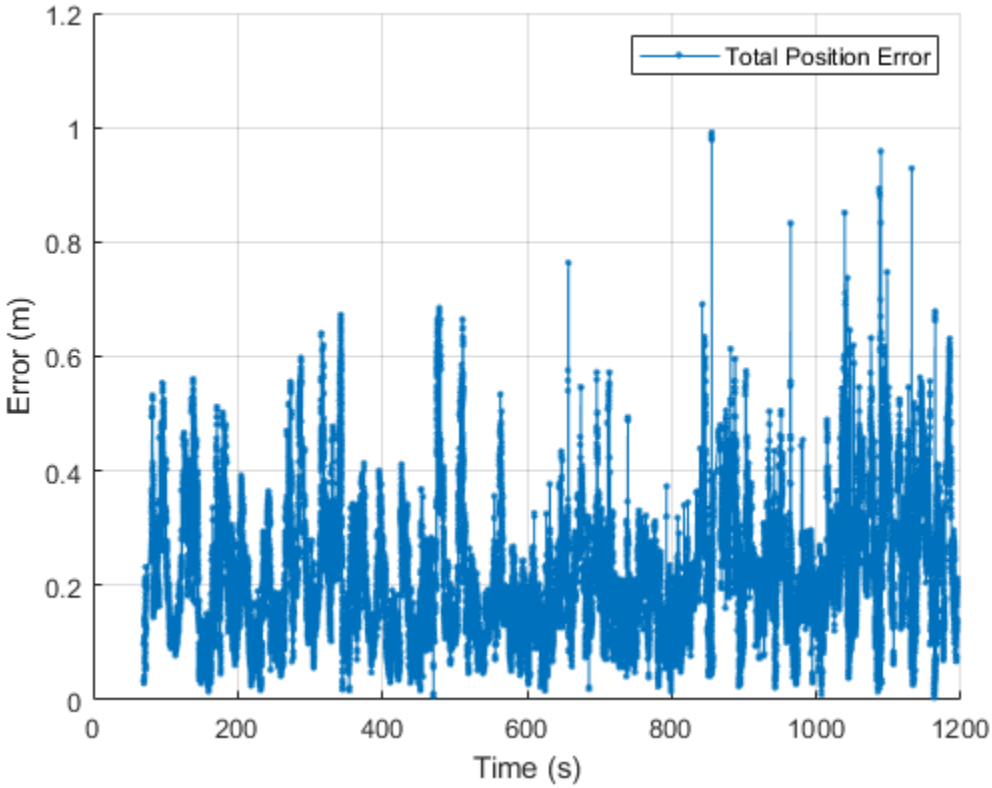

Fig. 13 3-D position-error magnitude (total position error) as a function of time for the position accuracy test data set

It is apparent from examination of the position-error components that the position error contains a small-magnitude high-frequency measurement noise component, as well as a position-bias error that varies more slowly as the UAS moves through the capture volume. The magnitude of this bias error is partially a function of the specific location of the marker within the capture volume. As the marker moves throughout the volume, the individual cameras detecting the marker changes, as does the geometry of the stereo-vision solution used to estimate the marker position. This effect can be seen in Fig. 14 by examining those portions of the capture volume associated with higher than typical position error.

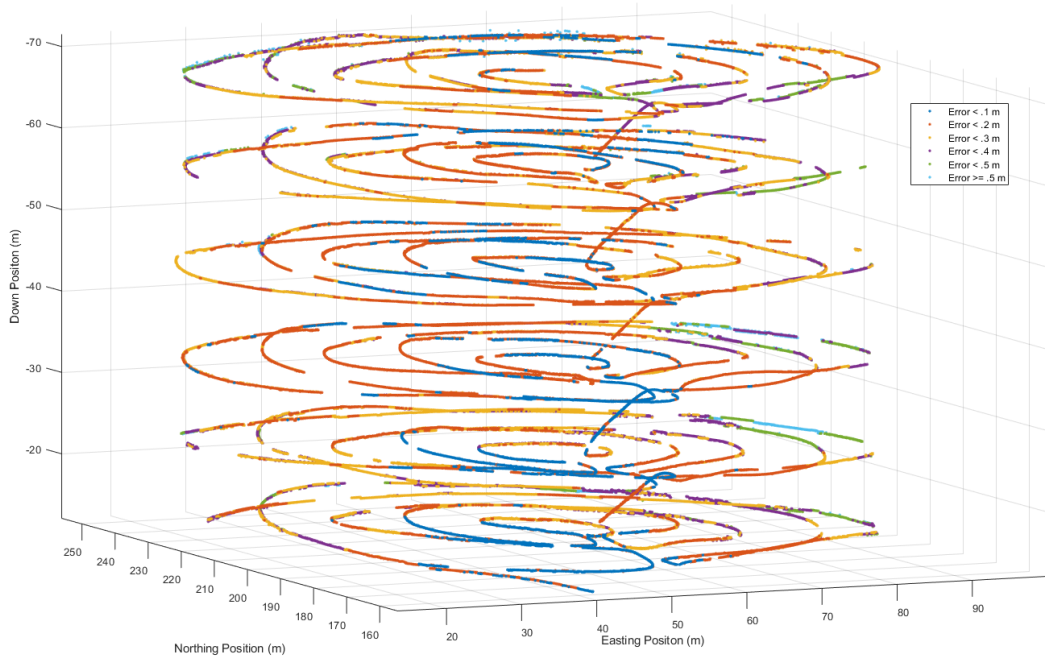

Fig. 14 Relationship between position-error magnitude and location of the marker within the capture volume

The position measurement rate of 100 Hz is relatively fast compared with the frequency content of the position flight dynamics of the UAS operating at a speed of approximately 5 m/s. Accordingly, it may be desirable to apply a low-pass filter to the position measurements in postprocessing to smooth the data and minimize the effect of the measurement noise. To investigate the effect of this approach on the measurement accuracy, a moving average filter with a filter window of 0.4 s duration was used to smooth out the raw position measurements from the motion-capture system. A plot of the total position error associated with this postprocessed data is shown in Fig. 15. Comparing this plot against Fig. 13, it is apparent that filtering the motion-capture data reduces some instances of momentary high position error. The largest position error observed for the raw data was 0.99 m compared with 0.67 m for the filtered position data. However, the majority of the position error is associated with position bias as the UAS moves throughout the capture volume and is not affected by applying a moving average filter to the raw data.

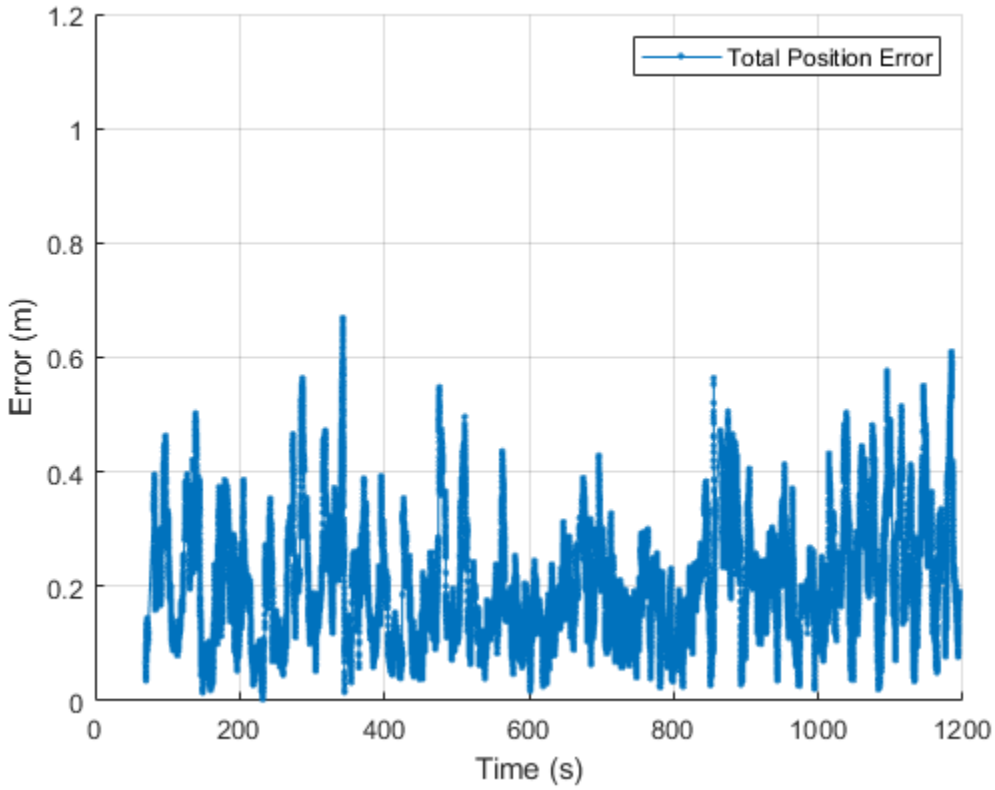

Fig. 15 Total position error as a function of time for motion-capture position measurements after a moving average filter was applied to the position measurements in an attempt to reduce measurement noise

Characterization of the overall position-tracking accuracy of the system for comparison against the established performance requirements requires a statistical assessment of the position error over the duration of the test event. Histograms of the orthogonal position error components for the entire measurement comparison data set are shown in Fig. 16.

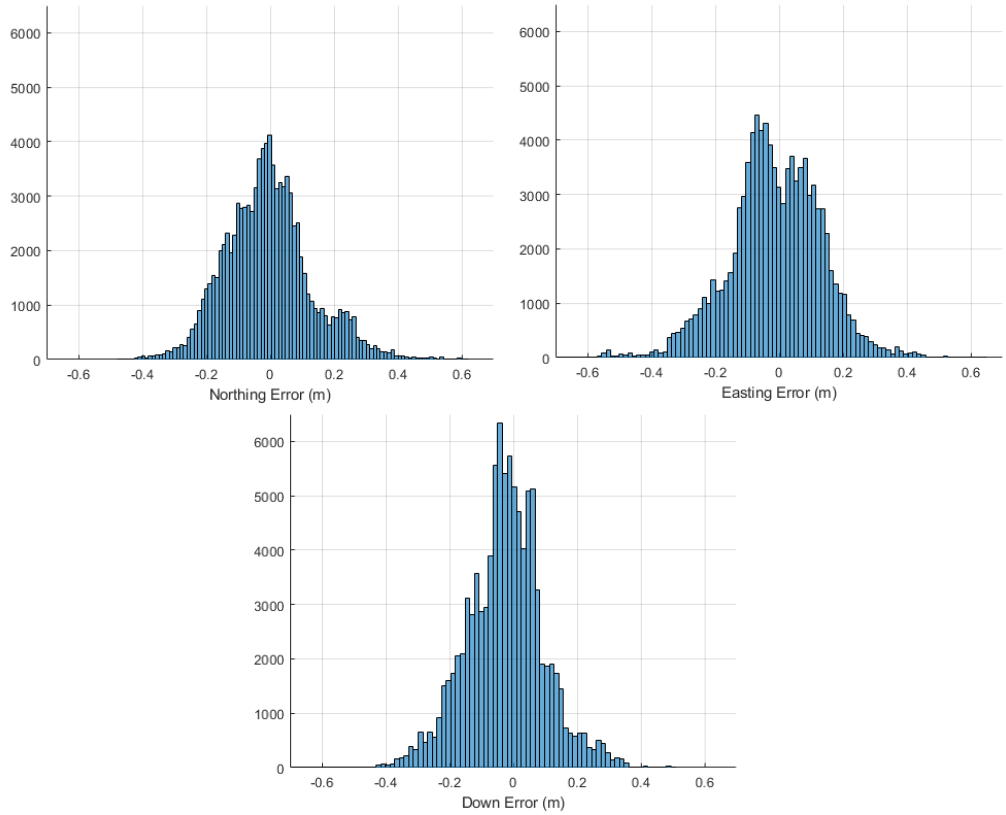

Fig. 16 Histograms of position error for each of the orthogonal components

A histogram of the total position error is shown in Fig. 17. The mean total position error was 0.207 m. Because the total position error is the norm of component errors in 3-D, it is appropriate to characterize this distribution as a chi distribution with 3 DOF, also known as a Maxwell–Boltzmann distribution. However, the quality of the fit for the Maxwell–Boltzmann distribution was less than desirable, as shown by Fig. 18. This is likely because the assumption that the all three error components are normally distributed with zero mean, and equal variance is not held true for this data set.

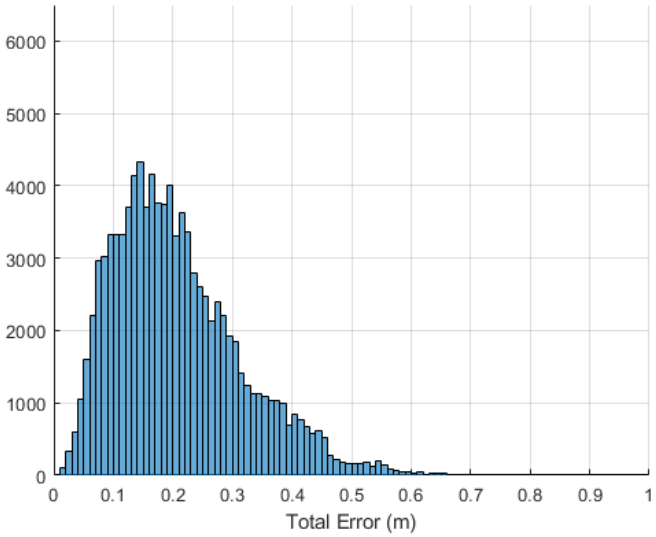

Fig. 17 Histogram of 3-D position error magnitude (total position error) for the position accuracy test data set

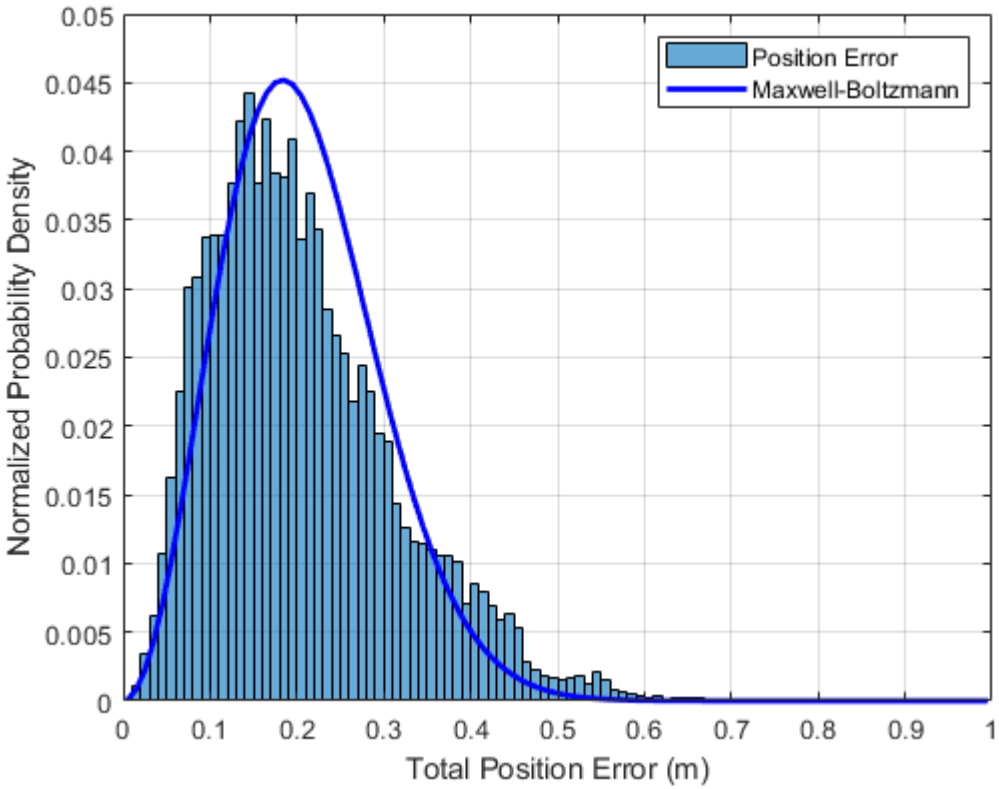

Fig. 18 Fit of Maxwell–Boltzmann probability density function to the position-error distribution

An alternative to characterizing the position-tracking accuracy with a probability distribution is to use spherical error probable (SEP) as the performance metric. This

metric refers to a sphere of given radius, centered on the true value, within which a certain percentage of the measurements occur. SEP is commonly used for characterization of the accuracy of navigation systems[17] and is similarly appropriate for this application. Commonly used percentile thresholds for calculation of SEP are 50% and 90%, referred to as SEP50 and SEP90, respectively.

The measurements collected during this test event exhibited an SEP50 value of 0.189 m and an SEP90 value of 0.362 m. It is also useful to use the threshold position-tracking accuracy requirement of 0.5 m, established by ARL as a performance benchmark. It was found that 98.6% of the observed measurements had less than this level of error. The demonstrated level of tracking accuracy exceeds the threshold requirement established for development of the system and is an impressive result for position tracking within a motion-capture volume of greater than 3 million m^3.

5.2 Discussion of Tracking Accuracy Error

It is useful to examine the instances of higher than typical position error to gain insight into specific scenarios that may be contributing to the position error. Figure 19 highlights a specific time period where a number of samples had position error greater than 0.6 m. Figure 20 depicts the component position errors for this specific time period of the test as a function of time. Figure 21 depicts the horizontal plane position estimate produced by the motion-capture system and the postprocessed ground truth data generated by the TS16.

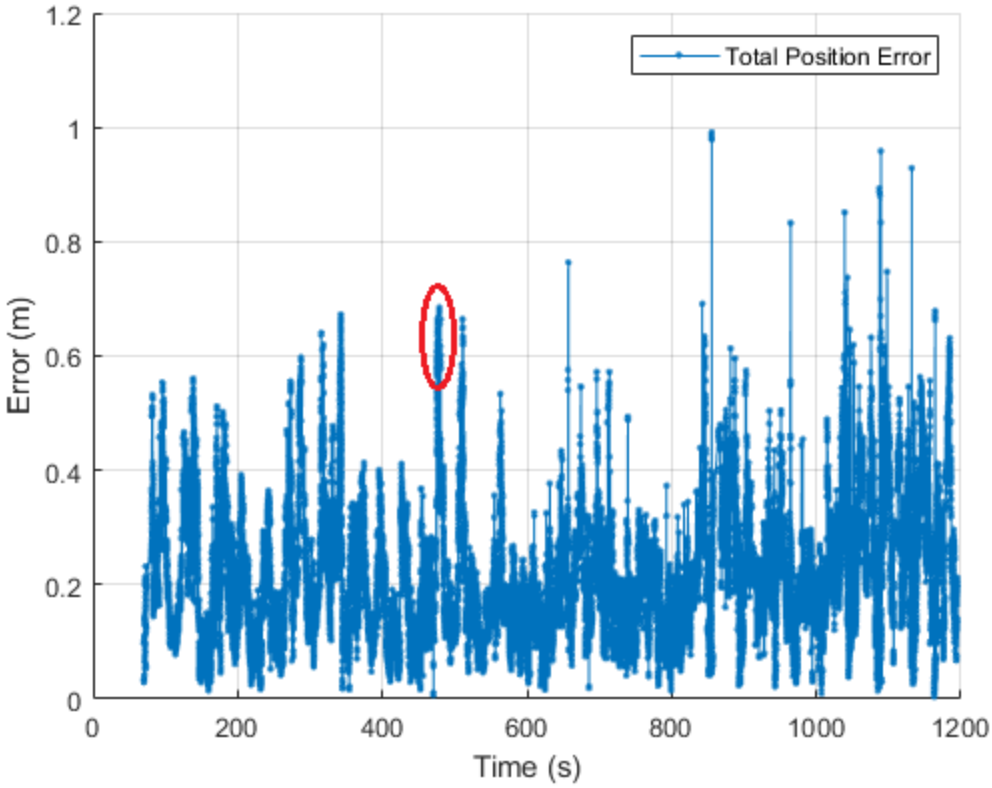

Fig. 19 Highlighted data segment with higher than typical position error

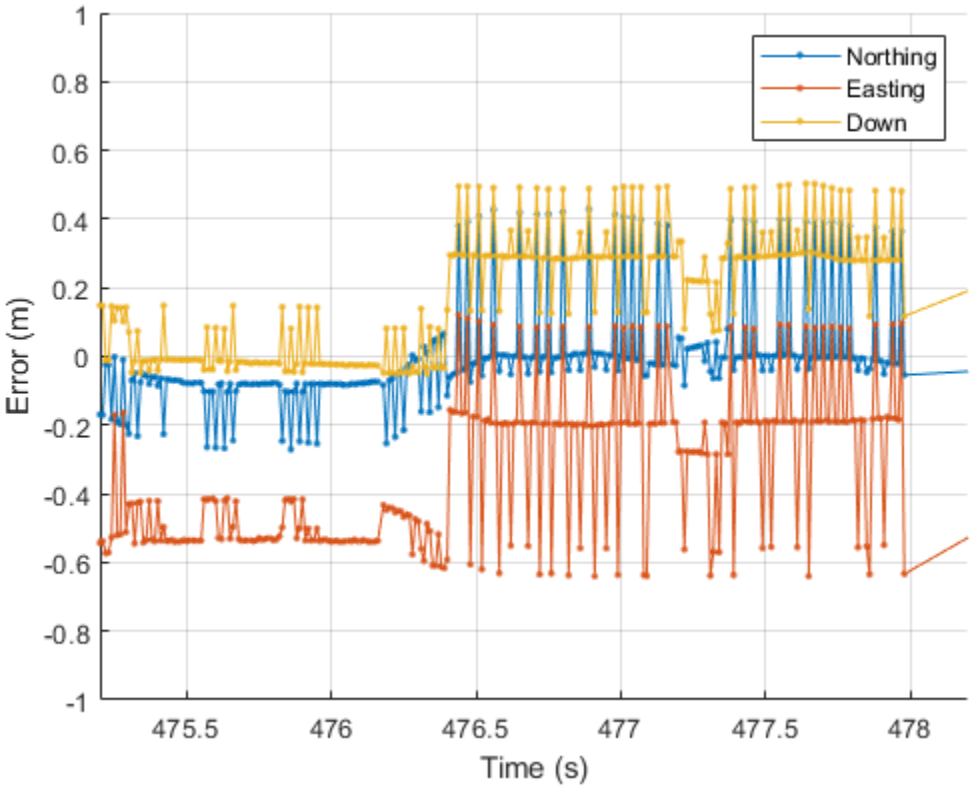

Fig. 20 Position error components for segment of data with higher than typical error

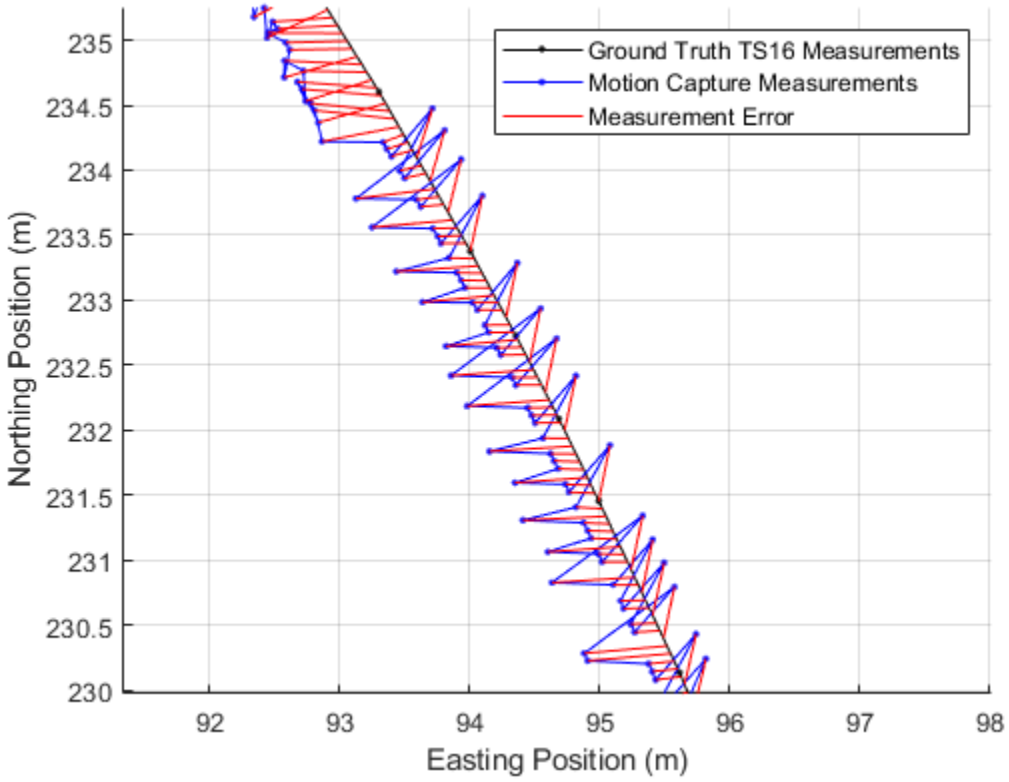

Fig. 21 Horizontal plane representation of motion-capture data, ground-truth position, and measurement error for a segment with higher than typical position error

Visualization of the camera rays indicating detection of the marker by a given tracking pod reveals that during the segment of time highlighted in Figs. 19–21, the number of tracking pods detecting the marker was frequently changing. The high-frequency measurement noise observed in this example is associated with instantaneous jumps in the estimated position when the number of tracking pods that contribute to the estimate changes. This characteristic of the marker-position measurements is consistent throughout the recorded data. When the number of tracking pods detecting the marker changes, the stereo-vision solution adjusts to the new number of inputs resulting in a jump in the position estimate.

Investigating the segment of higher than typical error further, it is apparent that for the specific instances of error greater than 0.6 m only two or three pods were detecting the marker. Often, one of these pods was located over 200 m from the marker. This scenario highlights a number of underlying factors associated with the accuracy of position estimates generated from computer stereo vision.

Generally, computer stereo vision relies on a calibrated camera model to characterize a projective transformation from the camera pixel space into the world frame. It also relies on a calibration of the system configuration to estimate the pose of each camera with respect to the local frame. Using these models, any pixel

location on the camera sensor represents a ray originating at the camera location and projecting into the world frame. In the case of a perfect camera model, an object detected by the sensor will lie somewhere along this camera ray in the world frame. Practically, however, error is introduced in the transformation between the sensor frame and the world frame. This error can be associated with the discrete resolution of the sensor, errors in the camera model, errors in estimation of the camera pose, or a combination of all these factors. Note that because the conversion from the sensor frame to the world frame is a projective transformation, any error in the model of this transformation results in error in the spatial coordinates of the world frame that increases linearly with the distance between the camera and the detected object.

Estimating the position of a detected marker requires that a minimum of two tracking pods detect the marker simultaneously. An optimization algorithm is used to estimate the location of the marker associated with the imperfect intersection of camera rays emanating from each camera that detects the marker. This optimization benefits from a perspective between cameras that is increasingly orthogonal according to the principles of dilution of precision. Increasing the number of cameras detecting the marker typically reduces the error in the estimated position by reducing the dilution of precision and providing additional inputs to the optimization algorithm. If the error associated with the contribution from each camera is assumed to be zero mean white noise of equal variance, the measurement error will decrease as additional observations are added to the optimization solution.

The current implementation of the motion-capture system uses an optimization algorithm for estimation of marker position that weights all observations equally in the solution. However, as described previously, the error associated with a given observation is expected to increase linearly with the distance between the camera and the marker. This is particularly noteworthy given the scale of the system and the ability of the cameras to detect markers at long distances. Markers were often detected by cameras up to 250 m away. Contributions from these instances are expected to contribute more than double the measurement error than a camera at a more typical detection range of 100 m. It is likely that the accuracy of the position measurements could be improved in the future by applying a weighting function in the optimization solution based on the range of the marker from a given camera.

Qualitative examination of specific segments of data from the test reveals results consistent with the practical limitations of a motion-capture systems based on stereo-computer vision. Measurements with low levels of total position error often had up to seven cameras detecting the marker, in a configuration producing a low dilution of precision, with limited distances between the cameras and the marker.

A representative example is shown in Fig. 22. Conversely, measurements with higher levels of total position error often result from few cameras detecting the marker and either a camera configuration producing an increased dilution of precision or large distances between the marker and some of the cameras contributing to the solution. Representative examples of these scenarios are shown in Figs. 23 and 24, respectively.

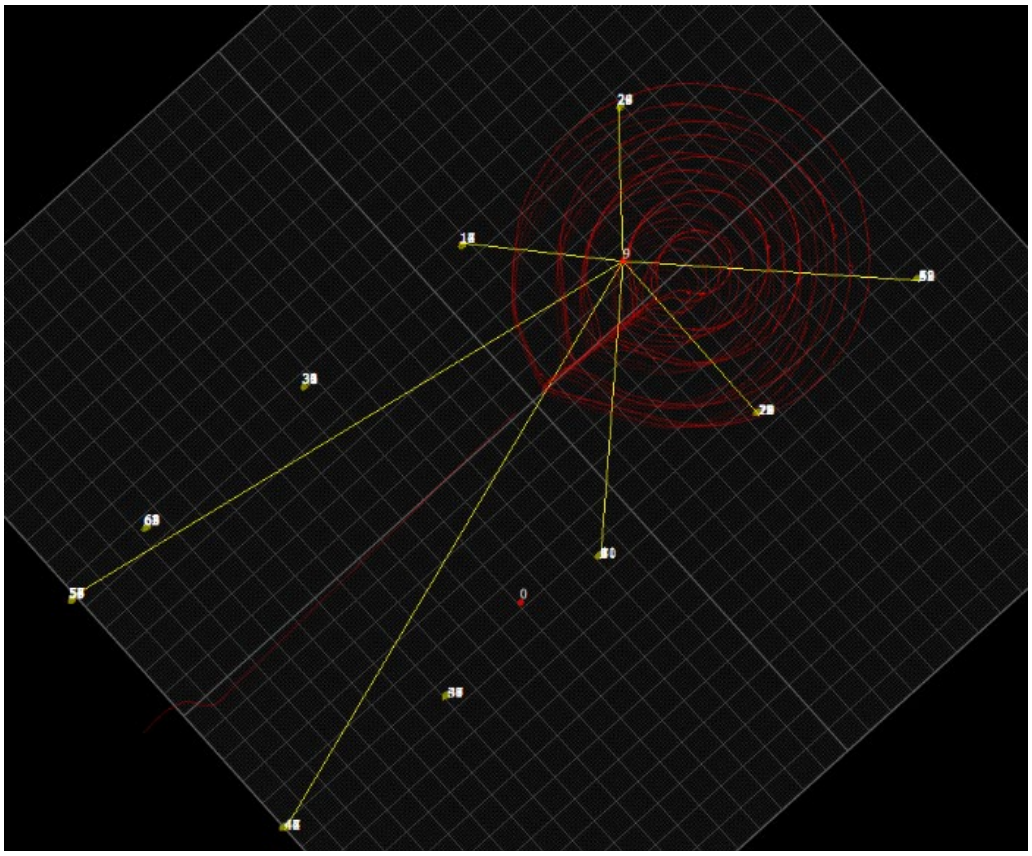

Fig. 22 Example marker detection scenario for a measurement with low position error

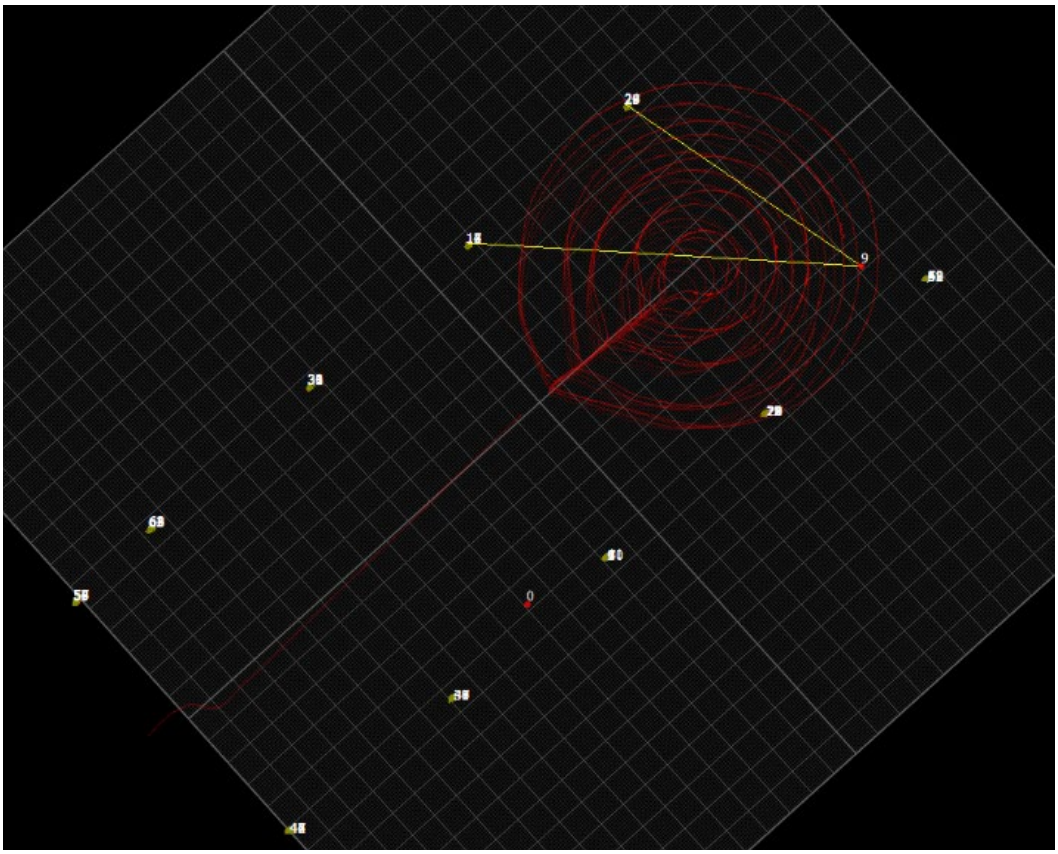

Fig. 23 Example marker detection scenario with few cameras detecting the marker and a relatively high dilution of precision resulting in high position error

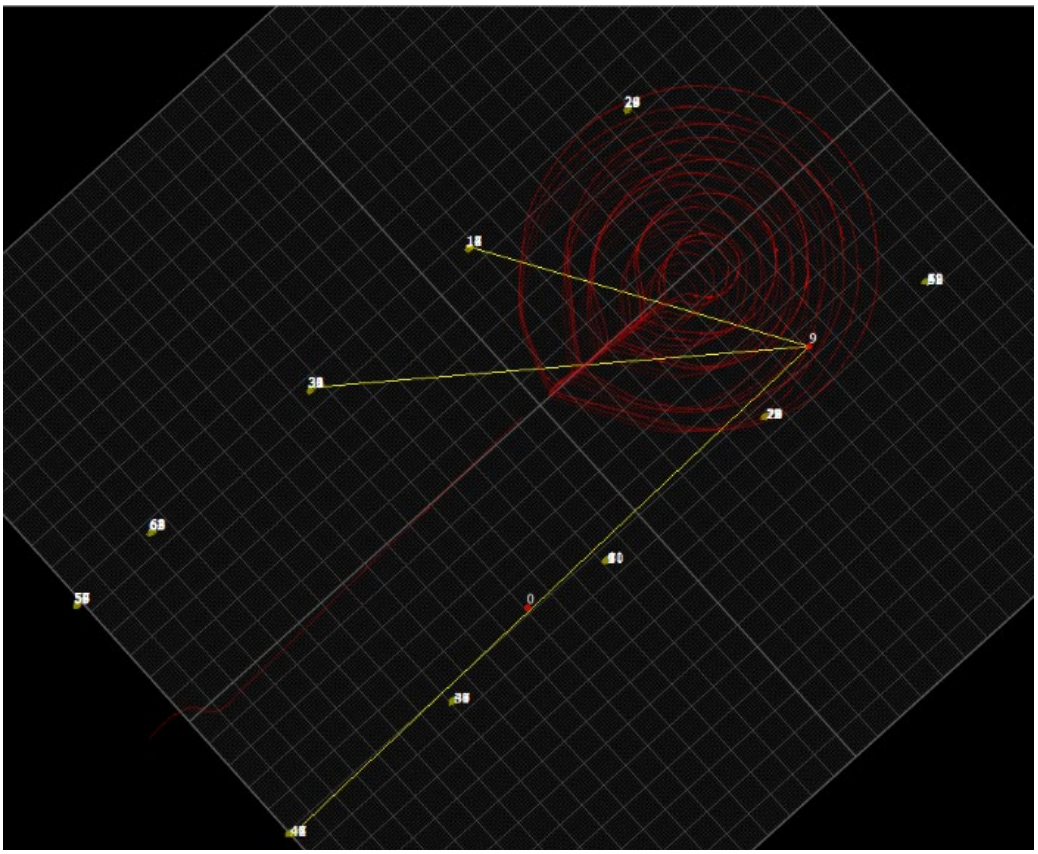

Fig. 24 Example marker detection scenario with few cameras detecting the marker and detection by a camera a long distance from the marker resulting in high position error

5.3 Evaluation of Position-Tracking Precision

The rigid, rotating-arm apparatus described in Section 4.4 was used to collect position measurements specifically for the purpose of evaluating measurement precision. The rotating arm was placed in a series of positions within the capture volume and manually spun for approximately 10 revolutions. Examination of these data segments reveals the same measurement characteristics as observed with the marker moved throughout the space by the UAS. When the number of cameras detecting the marker changes, the position estimate instantaneously shifts. However, when the number of cameras detecting the marker is stable, the planar circular motion is remarkably consistent. It is these periods of consistent measurement over multiple revolutions that are of interest for evaluating the measurement precision. A specific case was selected for detailed analysis. Six cameras were tracking the marker for the majority of the data points associated with this case, as shown in Fig. 25. This case represents the best-case measurement precision of the system because measurement noise associated with variation in the number of cameras detecting the marker has been eliminated.

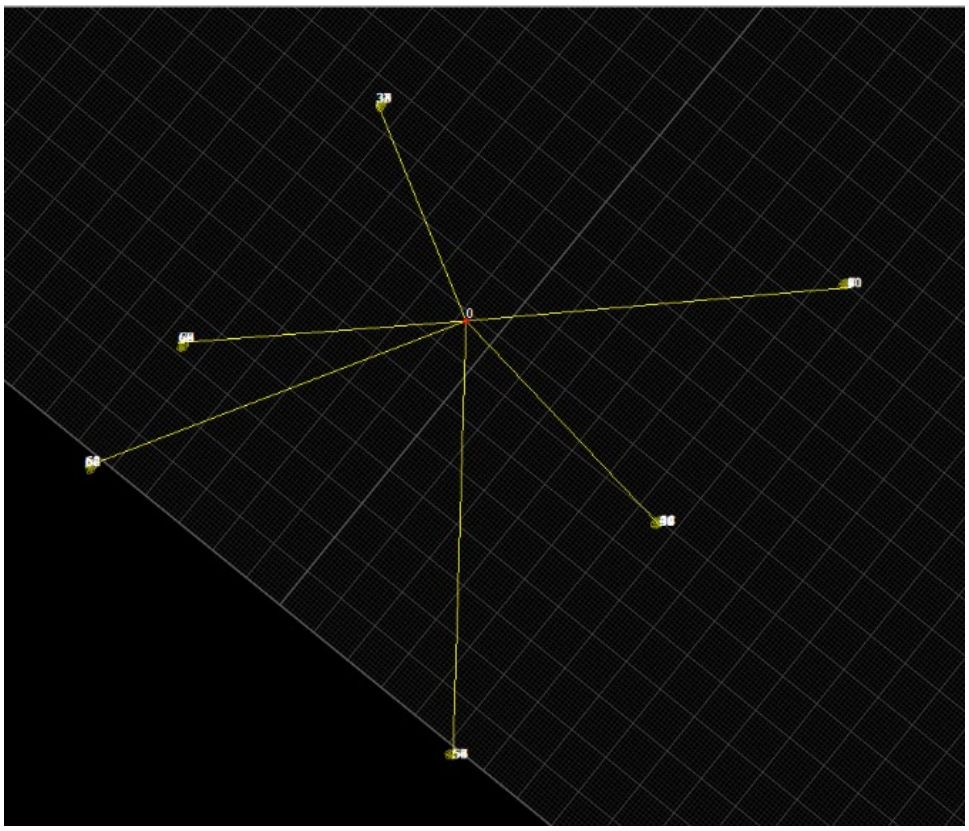

Fig. 25 Marker detection scenario used for evaluation of position measurement precision

The rigid rotating-arm apparatus generated repeatable, circular, planar motion of the marker with a radius of rotation of 2.28 m. It is possible to use this constrained geometry to generate a basis for evaluation of the precision of measurements from the motion-capture system. A custom optimization algorithm was used to establish a centroid and plane of rotation for the rotating arm of known radius, as shown in Fig. 26. Using only measurements when the number of cameras detecting the marker was stable, the magnitude of the error between this reference and the motion-capture position measurements characterizes the precision of those measurements, a best-case scenario for measurement precision of the system. A histogram of the measurement error is shown in Fig. 27. Using the same method to characterize this error distribution as described in Section 5.1, the mean error was 1.3 mm with an SEP50 of 1.1 mm and an SEP90 of 2.3 mm. Note that if the additional measurements from this segment of time are included, accounting for changes in the number of cameras contributing to the measurement, the mean error increases to 7.2 mm with an SEP50 of 1.4 mm and an SEP90 of 24.6 mm. To provide practical context for the level of precision achieved, Fig. 28 depicts a segment of the measured marker path in the horizontal plane. Note that the marker made 11 revolutions during this segment with the motion-capture system producing very repeatable results on each revolution.

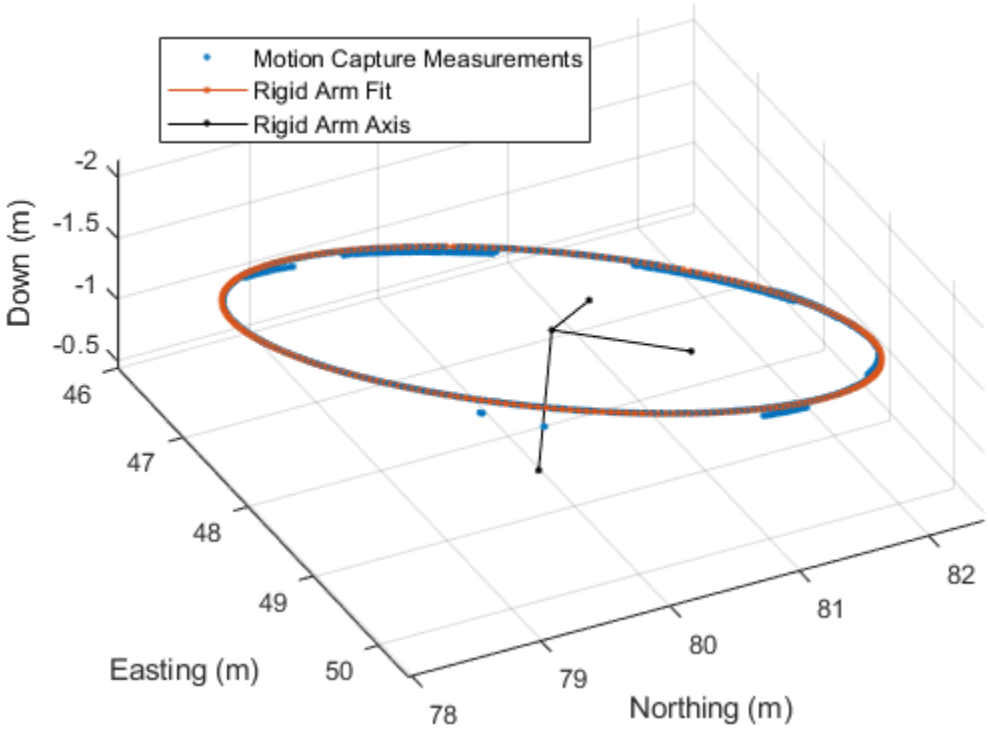

Fig. 26 Result of fitting a planar circular motion to position measurements associated with the rigid rotating-arm apparatus

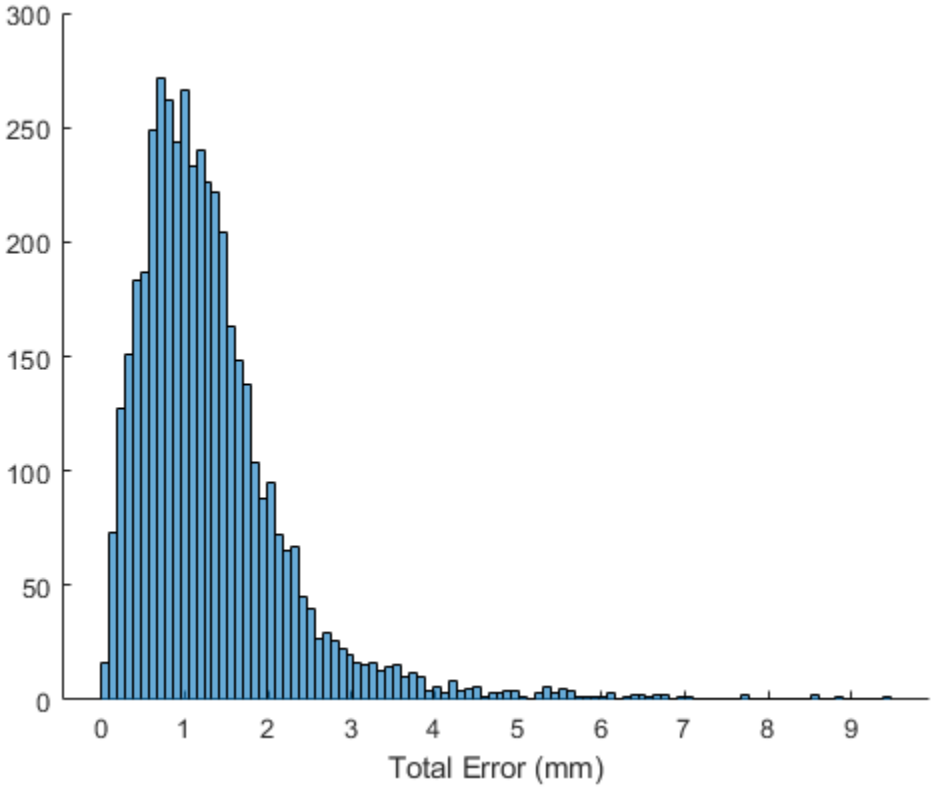

Fig. 27 Distribution of error between position measurements associated with the rigid rotating-arm apparatus and the planar circular motion fit best-case scenario

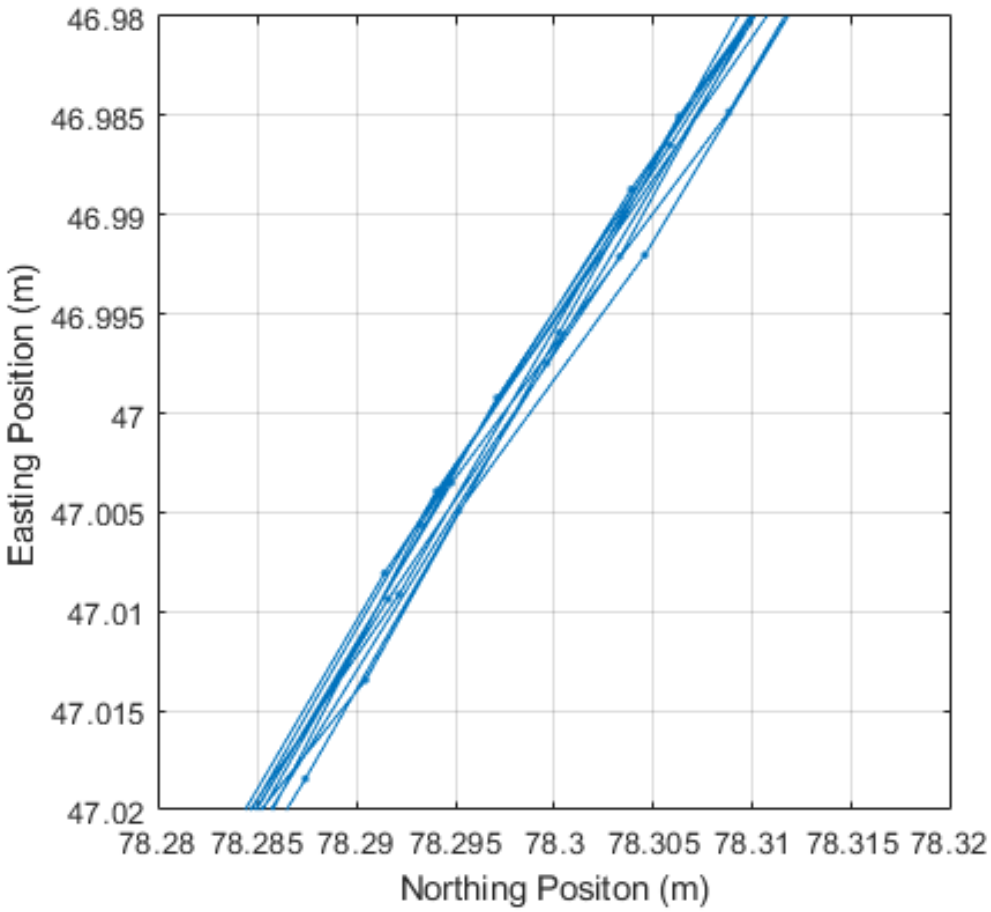

Fig. 28 Measurement precision of the motion-capture system was demonstrated by the consistency of position measurements associated with the rigid rotating-arm apparatus

5.4 Demonstration of Tracking a Projectile Configuration

The manually launched projectile with integrated marker described in Section 4.5 was used to verify the ability of the system to track a marker in this configuration. This projectile was also able to achieve greater flight speeds than possible with the UAS, increasing the velocity at which the system's tracking performance was verified. The projectile was launched repeatedly at various locations throughout the motion-capture volume, as shown in Fig. 29. The flight path was primarily along the longitudinal axis of the capture volume, as would be typical for an actual flight experiment. Eight projectile flights were captured in this data set. The motion-capture system was able to successfully track the projectile for each of the eight flights. Note, however, that a gap in the tracking solution exists just after launch in each example. A single case Fig. 30 was selected for more-detailed analysis.

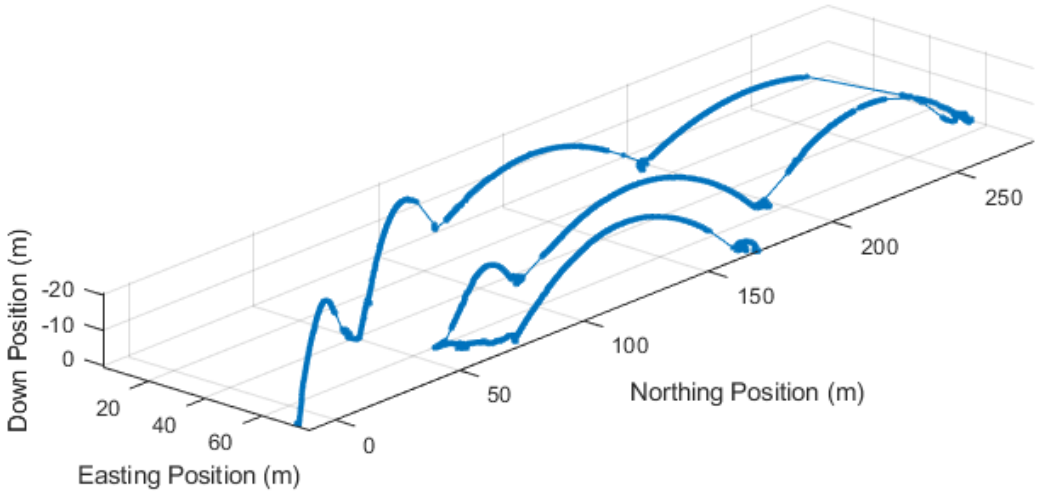

Fig. 29 Series of trajectories for a manually launched projectile with an integrated tracking marker

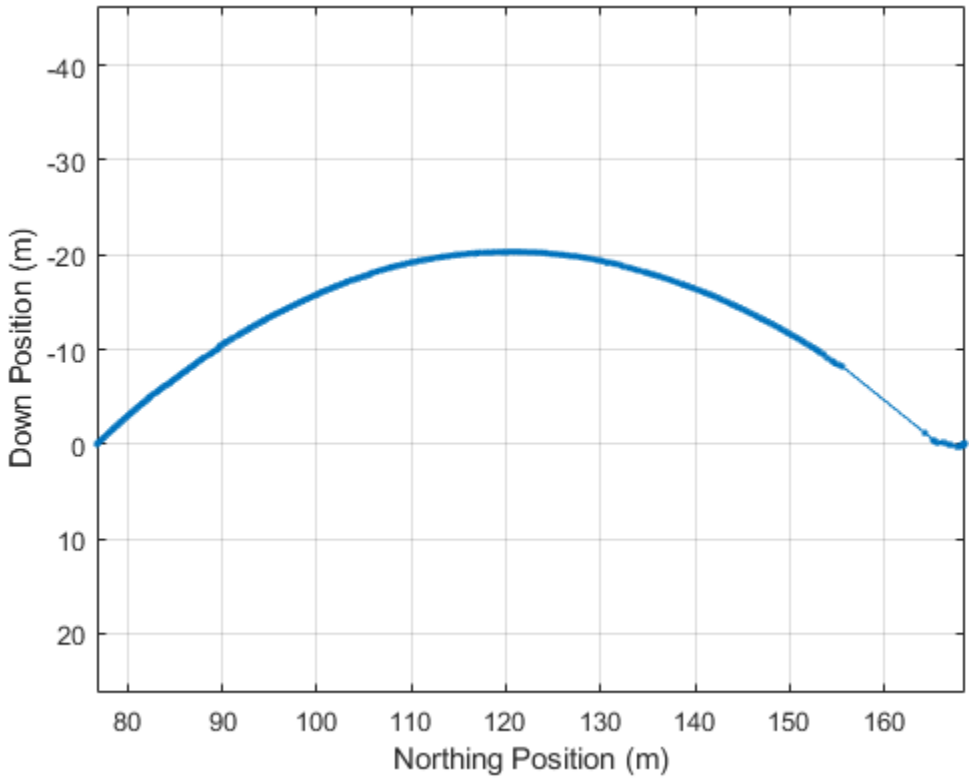

Fig. 30 Trajectory profile of manually launched projectile selected for detailed analysis (direction of travel is from right to left)

A point-mass ballistic model of the projectile trajectory including acceleration due to gravity and aerodynamic drag was created to approximate the projectile flight dynamics. The drag coefficient and initial conditions for this model were manually

fit to the motion-capture data to provide a clean representation of the projectile flight path. The results of this process to approximate the flight path is shown in Fig. 31. The launch velocity estimated by the model is 33 m/s. Using the model to approximate the launch time, it appears that the gap in the motion-capture position-tracking solution was 360 ms.

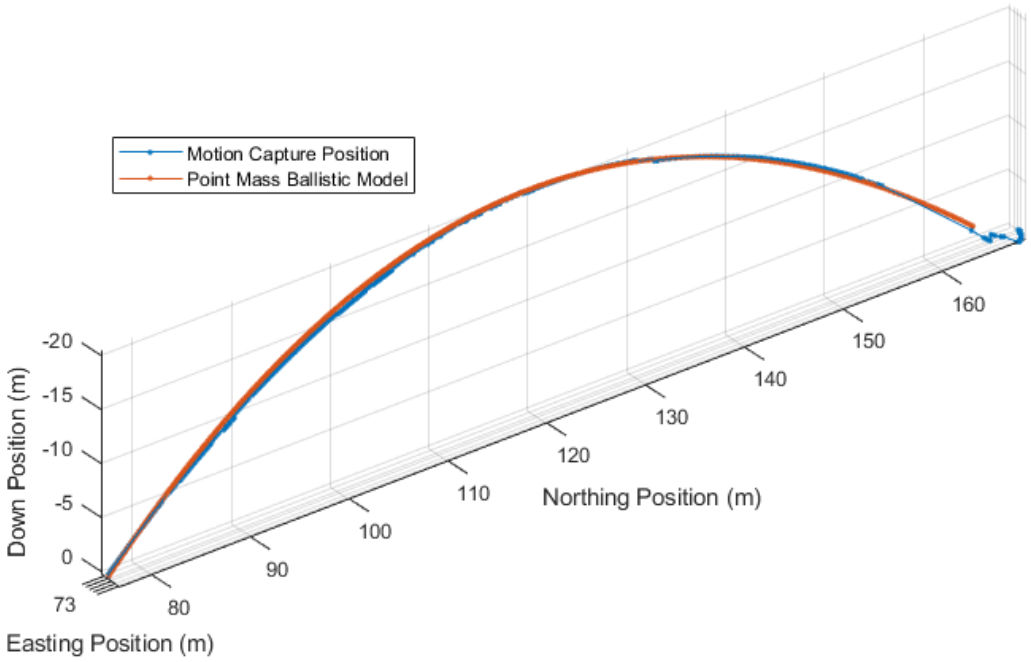

Fig. 31 Fit of point-mass ballistic model to trajectory profile captured by the motion-capture system

This gap in the tracking solution raises a concern that the motion-capture system is incapable of tracking markers at velocities over approximately 30 m/s. Engineering analysis of the camera integration time and the spatial resolution of the cameras at functional ranges suggest that the system should be capable of tracking markers at velocities exceeding 100 m/s. Examination of individual frames from cameras that should have been tracking the projectile during the interval in question revealed that the cameras were detecting the marker but were not able to extract the identification code of the marker from the modulation of strobe intensity. It is speculated that rapid pitching motion of the projectile just after launch caused by the dynamics of the trebuchet launch method generated an apparent variation in the marker brightness when detected by the cameras. This unexpected variation in marker intensity may have kept the cameras from properly identifying the marker code until the pitching motion damped out. It is not possible to definitively state the cause of the gap in the ability of the system to identify the marker code from the currently available data, and additional testing will be required if this system response is deemed unacceptable for specific test events. Even though the marker

was not identified in near-real time during the tracking gap, because the marker was detected throughout the gap, the flight path of the projectile can be recreated in postprocessing if desired.

The demonstration of a marker integrated into a surrogate projectile demonstrated that this configuration is a viable capability of the system. Motion capture of the projectile flight path in near-real time with positive identification of the marker code was demonstrated up to 30-m/s projectile velocity. Marker detection without marker code identification was demonstrated up to 33 m/s. It is expected that the previous engineering analysis predicting tracking performance of markers exceeding 100 m/s is still valid, although this performance has not been verified simply because it is difficult to practically achieve higher velocities without a more-advanced projectile launcher.

5.5 Performance Criteria Not Directly Evaluated

Some of the performance criteria established by ARL could not be directly evaluated as part of the test event. These system-performance characteristics must either be evaluated through engineering analysis of the system design or through indirect observation.

As discussed in Section 5.4, the ability of the system to track a marker moving at high speed was demonstrated up to a marker velocity of 33 m/s. It was not feasible to achieve higher marker velocities to directly observe tracking performance up to the objective requirement of 100 m/s. Engineering analysis predicts the ability to track markers at velocities exceeding this requirement. During system development, PhaseSpace performed a test to rapidly sweep a marker across the pixel space of a camera as an approximation of tracking a marker moving at high speed in the spatial domain. This test involved rapidly slewing a camera past a fixed marker, which verified the ability of the camera to track a marker rapidly transiting the camera pixel space. The maximum speed for a marker moving through the capture volume at which the system can generate valid position measurements remains unverified.

ARL specified that the motion-capture system must be capable of generating position measurements of a marker in near-real time. Quantitative characterization of the measurement latency would require a specific hardware configuration to log the timing of camera exposures and position measurement solutions on a common time base. This effort is outside the scope of the current test and would need to be pursued in the future if specific uses of the motion-capture system require an accurate characterization of the measurement latency. Engineering analysis of the

system in its current configuration predicts measurement latencies of less than 30 ms.

ARL specified a requirement to simultaneously track at least 10 markers, with an objective requirement of 100 simultaneous markers. Testing conducted thus far has demonstrated simultaneous tracking of only three markers, limited by the availability of marker hardware. The bit length of the code broadcast by each marker using modulation of the marker brightness allows for up to 64 simultaneous marker codes. Additional simultaneous markers would be possible by extending the bit length of the code. While the capability for detection of many simultaneous markers remains unverified, it is expected that the system would track 64 markers without issue.

ARL specified the ability to capture the attitude of a vehicle as an objective requirement. The software provided by the tracking server has the ability to define rigid bodies represented by an array of three or more markers. Once a rigid body has been defined, the system is capable of estimating the attitude of a rigid body by simultaneously tracking the markers associated with the rigid body. This approach has been demonstrated by PhaseSpace on indoor motion-capture systems using software nearly identical to that implemented for the outdoor motion-capture system. The limiting factor in implementing this approach for the larger scale of the outdoor system is the requirement to position the multiple markers on the vehicle at sufficient separation from each other to produce adequate angular resolution for estimation of vehicle attitude given the spatial resolution of the motion-capture system. It is expected that the system is capable of estimating vehicle attitude, although this feature has not been explicitly tested. The accuracy of any attitude measurements generated by the system in the future would be a function of the position-measurement precision and accuracy for individual markers comprising a rigid body as well as the separation distance between those markers.

The ability of the system to disambiguate multiple markers located in close proximity is an important capability of the system if future tests are to evaluate concepts with low-separation distance between agents or configurations with multiple markers on a single agent. This capability was not explicitly characterized during the test event presented in this report. However, an alternative configuration of the rigid rotating-arm device was used to make qualitative observations on scenarios where multiple markers may obscure each other. A second marker strobe was added to the apparatus part-way between the pivot and the marker on the end of the rotating arm, resulting in a separation distance of 1 m between markers. When rotated in the horizontal plane this configuration produces a situation where the two markers are momentarily aligned from the perspective of certain tracking

pods. By replaying data captured during this scenario it is possible to observe instances when the two markers rotate such that they are nearly aligned, as shown in Fig. 32. As they continue to rotate, the markers come into alignment from the perspective of a certain pod, resulting in the detection of both markers being lost, as shown in Fig. 33. As the rotating arm continues forward, the markers move out of alignment and are once again detected by the tracking pod, as shown in Fig. 34. Note that after the markers can be once again distinguished from each other, it takes a series of frames for the system to reestablish the code uniquely identifying each marker from the intensity modulation of the marker strobe. In the current configuration, this process can take up to 11 data frames, a duration of 110 ms. The sequence of tracking/lost detection/reacquisition repeats itself as the orientation of the arm results in marker alignment from the perspective of other pods as the arm advances forward. Because each tracking pod observes the markers from a different perspective, this scenario of lost marker detection occurs at different times for each pod. The overall result is that even though marker tracking is briefly lost for individual pods, the motion-capture system as a whole is able to continuously track the position of both markers without any gaps in the data.

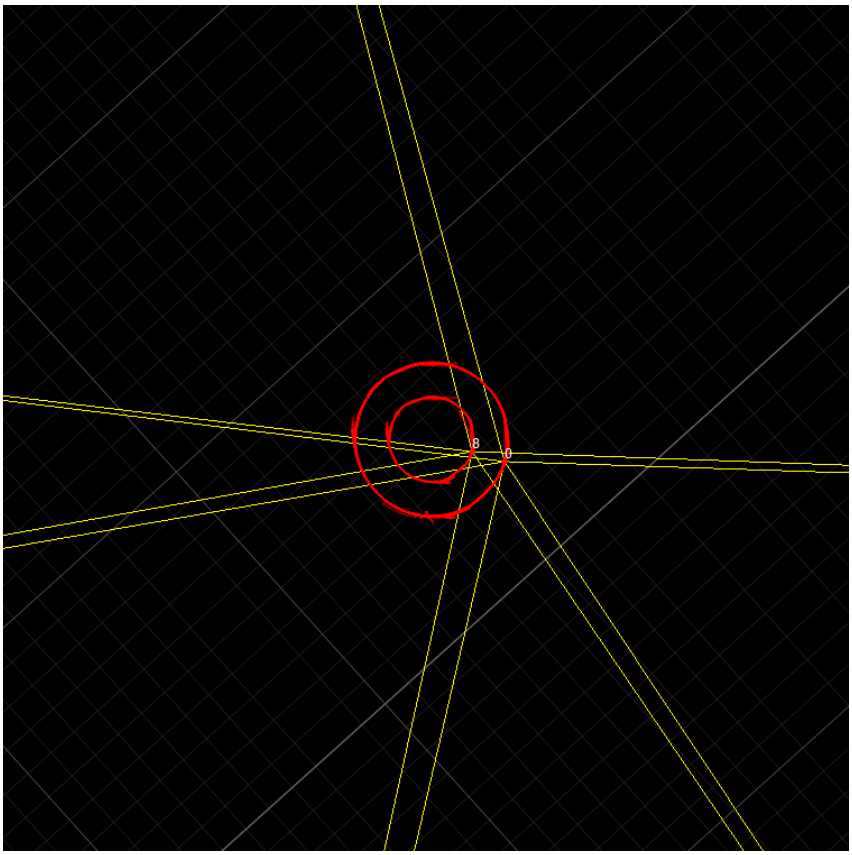

Fig. 32 Configuration of camera rays tracking two markers mounted on a rigid rotating arm. Counterclockwise rotation of the arm will result in loss of marker detection by cameras to the left and right shortly after this frame.

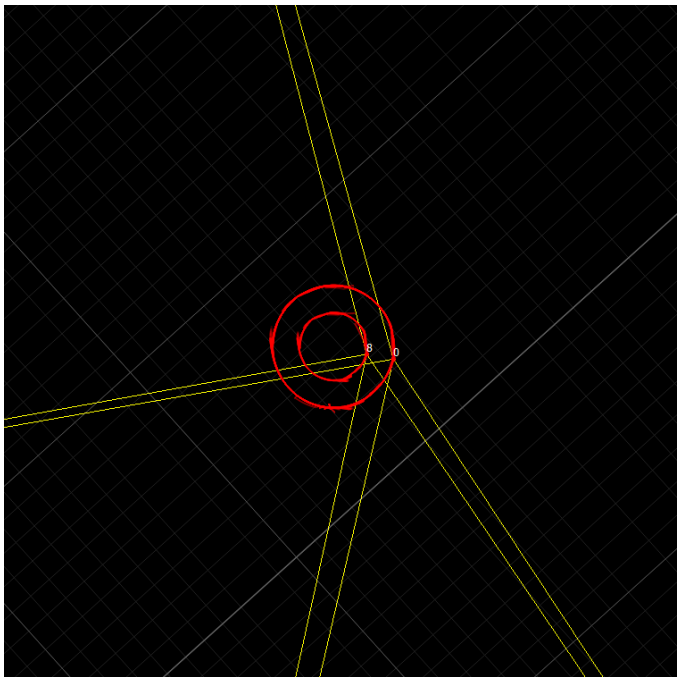

Fig. 33 Configuration of camera rays tracking two markers mounted on a rigid rotating arm. Position of the two markers has overlapped from the perspective of cameras on the right and left, resulting in loss of marker detection by those cameras.

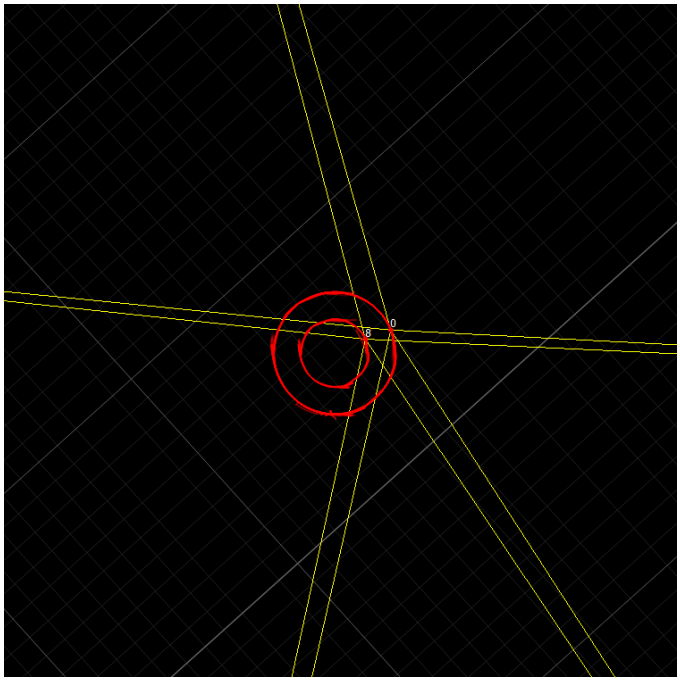

Fig. 34 Configuration of camera rays tracking two markers mounted on a rigid rotating arm. As the arm has continued rotating counterclockwise the position of the two markers has once again become distinct from the perspective of cameras on the right and left, resulting in reacquisition of the markers by those cameras.

5.6 Practical Considerations and Opportunities for Improvement

In addition to the quantitative assessment of measurement accuracy discussed, the test event provided an opportunity to evaluate the practical elements of successfully implementing such a large-scale complex motion-capture system. Specific elements of the system design as well as the configuration for this specific test event highlighted a need for several improvements, which will be pursued as the system is employed for test events supporting ARL research efforts.

The most-notable issue impacting the ability to efficiently collect data with the motion-capture system was poor reliability of network connections between tracking pods in the daisy-chain configuration. Because the data from pods toward the end of the chain pass through the network switch on several other pods, the configuration creates a "weakest link" scenario. If any interpod network connection fails, it is likely that the connectivity to multiple pods will be lost. This situation is exacerbated by the fact that the pods are located hundreds of meters from the command center of the experiment, requiring significant time and physical effort to just simply reset a pod. For unknown reasons, multiple failures of the network cables supplied with the system resulted in significant time spent debugging cable issues during the test event presented in this report. Replacing these cables with stock that ARL happened to have on hand seemed to resolve the issues. It is recommended that all of the current network cables be replaced with a ruggedized versions prior to future testing. It is also recommended that future iterations of the tracking pods be redesigned to allow for easier network troubleshooting.

The current aluminum pod stands with adjustable feet adequately serve the intended purpose of providing a base for the tracking pods that can be leveled to adjust for uneven ground at the designated test range. However, there is significant room for improvement in this element of the system design. The adjustment range of the stand's feet is small and difficult to manipulate. This design limits the degree to which unlevel ground can be accommodated. These stands are also less rigid than would be ideal for an application that relies on robust, rigid placement of high-resolution imaging devices. A mounting system based on the use of heavy-duty survey equipment tripods would address these concerns and result in a design that is both easier to set up and more robust once established.

One of the realities of such a large capture volume is the scope effort required to calibrate the system. A 20+-min-long UAS flight is required to generate calibration data and that data takes tens of additional minutes to process once collected. It is impractical to recalibrate the system frequently, and performing this process once at the start of each test day is the desired level of calibration effort. It is difficult,

however, in the current configuration to verify that a previously generated system calibration is still valid. It is possible for a pod to be bumped by personnel working on the system or disturbed by wind. These scenarios would invalidate the current calibration solution, but there is currently no method to verify the calibration health of the system. Because the detection range of the cameras is adequate to detect markers located across the width of the capture volume and beyond, it would be possible to place markers on each tracking pod and have them be detected by other tracking pods. Adding these static markers as a fiducial for monitoring calibration health would allow the system to identify a pod that had been bumped because the static markers would no longer be at the pixel coordinates they were detected at during the calibration. It is likely that these static markers located at known surveyed locations would also provide data to constrain the calibration solution, resulting in more-accurate calibration solutions.

The intrinsics models of the cameras located within each tracking pod were recalibrated during the week prior to the test event discussed in this report. This calibration process consists of mounting each tracking pod on a pan/tilt apparatus, capturing a series of images of a checkerboard pattern displayed on a large flat-screen television, and processing the resulting imagery to characterize each camera. This sequence is labor-intensive and requires approximately 1 h of effort for each pod. The accuracy of this calibration is critical to the overall motion-capture position-tracking accuracy. However, the stability of this pod intrinsic calibration over time is unknown. As the tracking pods are handled multiple times during transportation, setup, and breakdown, it is possible that the detailed properties of the projective transformation associated with each camera could change slightly due to vibration and shock. It is also possible that the calibration of the cameras could vary with temperature. The stability of camera calibration has not been assessed, and to do so would require a significant investment in resources. In lieu of a more-comprehensive understanding of this effect, the age of camera intrinsics calibration data must be considered as an element of system usen in support of future test events. Spot checking of system measurement accuracy using survey equipment is probably justified as an element of each test.

6. Conclusion

ARL has implemented the world's largest outdoor motion-capture system using hardware and software custom-designed by PhaseSpace, Inc. This system demonstrated the ability to meet the established performance requirements during a recent test. The motion-capture system captured position measurements for a marker mounted on a UAS with a position-tracking accuracy SEP50 value of 0.189 m and an SEP90 value of 0.362 m. Marker tracking was demonstrated over

a motion-capture volume exceeding 3 million m^3. Tracking position precision was observed to be as good as 1.3 mm in cases where the number of cameras detecting a marker was stable. Position tracking of a marker integrated into a surrogate projectile configuration demonstrated tracking of the marker at velocities up to 33 m/s. Over the course of the test event, cameras within the tracking pods were able to reliably detect active marker strobes at ranges exceeding 150 m and often detected markers as far away as 250 m. This ability to track markers at extreme ranges for a motion-capture system suggests the possibility of establishing even larger capture volumes than demonstrated thus far.

Minor issues associated with system reliability and practical implementation for efficient testing still exist, but it appears that PhaseSpace has solved the major technical barriers that have previously prevented outdoor optical motion-capture at the scale that is now possible with this system. ARL intends to continue to refine and resolve remaining limitations of the system as resources become available.

The capability to perform motion-capture measurements of large-scale outdoor test events promises to advance multi-agent collaborative navigation technologies by enabling ARL to conduct experiments that were not previously possible. This capability also has the potential to advance other ARL research areas involving the interaction of multiple moving agents. These areas include but are not limited to heterogeneous swarming concepts, ground/aerial agent interactions, counter-UAS systems, and human–agent teaming.

7. References

1. Allik BL, Hamaoui M, Don M, Miller C. Kalman filter aiding MDS for projectile localization. Presented at the AIAA Scitech 2019 Forum; 2019 Jan 7–11; San Diego, CA.

2. Hamaoui M. Non-iterative MDS method for collaborative network localization with sparse range and pointing measurements. IEEE Transactions on Signal Processing. 2019;67(3):568–578.

3. Bregler C. Motion-capture technology for entertainment. IEEE Sig Proc Mag. 2007;24:160–158.

4. Mellinger D, Michael N, Kumar V. Trajectory generation and control for precise aggressive maneuvers with quadrotors. Int J Robotics Res. 2012;31(5)664–674.

5. Michael N, Mellinger D, Lindsey Q, Kumar V. The GRASP multiple micro-UAV testbed. IEEE Rob Autom Mag. 2010;17(3):56–65.

6. Kushleyev A, Mellinger D, Powers C, Kumar V. Towards a swarm of agile micro quadrotors. Auton Robots. 2013;35(4):287–300.

7. Preiss JA, Honig W, Sukhatme GS, Ayanian N. Crazyswarm: A large nano-quadcopter swarm. Proceedings of the IEEE International Conference on Robotics and Automation; 2017 May 29–June 3; Singapore.

8. Godil A, Tsai R, Hong H. Ground truth systems for object recognition and tracking. Gaithersburg (MD): National Institute of Standards and Technology, Department of Commerce (US); 2013 Mar. Report No.: NISTIR 7923.

9. Jud D, Michel A. Motion tracking systems: an overview of motion tracking methods. Studies on mechatronics. Zurich (Switzerland): Swiss Federal Institute of Technology Zurich; 2011.

10. Don ML. The feasibility of radio direction finding for swarm localization. Aberdeen Proving Ground (MD): Army Research Laboratory (US); 2017 Sep. Report No.: ARL-TR-8114.

11. Lockspeiser JR, Don ML, Hamaoui M. Radio frequency ranging for swarm relative localization. Aberdeen Proving Ground (MD): Army Research Laboratory (US); 2017 Oct. Report No.: ARL-TR-8194.

12. Don ML. Dilution of precision as a geometry metric for swarm relative localization. Aberdeen Proving Ground (MD): Army Research Laboratory (US); 2017 Nov. Report No.: ARL-TR-8200.

13. Grabner M, Don M, Everson D. Constrained geometry relative swarm localization. Aberdeen Proving Ground (MD): Army Research Laboratory (US); 2017 Dec. Report No.: ARL-TR-8877.

14. McSheery TD, Black JR, Nollet SR, Johnson JL, Jivan VC, inventors; Phasespace, Inc., assignee. Distributed-processing motion tracking system for tracking individually modulated light points. United States patent US 6,324,296. 2001 Nov 27.

15. Ryer AD. Light measurement handbook. Peabody (MA): Light Technologies, Inc.; 1997.

16. Leica Geosystems. Leica Viva TS16 – world's first self-learning total station [accessed 2020 Feb 24]. https://leica-geosystems.com/en-us/products/total-stations/robotic-total-stations/leica-viva-ts16.

17. Ignagni M. Determination of circular and spherical position-error bounds in system performance analysis. J Guid Control Dynam. 2010;33:1301–1305.

Appendix. Method for Correcting Timestamp Errors of Leica TS16 Total Station Data

The survey data collected during the test event by the Leica TS16 were intended to be used as natively recorded for ground-truth position of the tracking marker. However, as discussed in Section 5.1 of the main report, it was determined after the conclusion of the test that the timing accuracy of the raw TS16 measurements was insufficient for evaluation of the position-tracking accuracy of the motion-capture system.

Examination of the recorded data in conjunction with information received from Leica technical support identified that the position values of collected measurements are valid within the accuracy of the instrument even though the timestamps associated with those measurements are inaccurate. This effect can be seen in Fig. A-1. In the top panel, the position of the survey prism as a function of time exhibits the timing errors associated with the TS16 measurements, resulting in a "noisy" position trace even though the UAS was flying in a smooth arc. In the bottom panel, this smooth flight path is apparent by plotting the position of the UAS in the horizontal plane independent of time for the same segment.

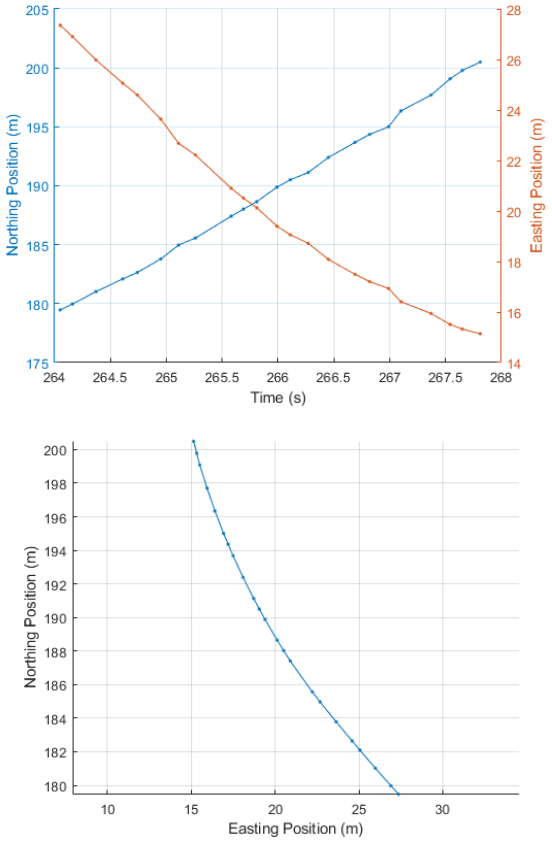

Fig. A-1 Segment of raw data recorded by the TS16 displayed both as a function of (top) time and (bottom) in the horizontal plane to demonstrate the effect of timing errors for position measurements that are otherwise accurate

Using the assumption that position values for the TS16 measurements are accurate and only the timestamps contain error, local-time corrections can be made if the velocity of the UAS is known. Position measurements from the motion-capture system covering the same time period as the TS16 measurements can be used to provide the necessary velocity input. It is undesirable to use the motion-capture measurements for manipulating the TS16 measurements because this approach has the potential to bias the ground truth in such a way as to minimize the position error calculated in assessment of the motion-capture system performance. However, alternate sources of the necessary data are not available, and the timestamp correction algorithm has been designed to minimize the impact of using the motion-capture data as an input. In addition to the assumption that only the timestamps of the TS16 data are flawed, the following assumptions were leveraged in creation of the timestamp correction algorithm:

1) The UAS was flying a circular pattern at a generally constant airspeed. The design of the flight plan in conjunction with the flight dynamics of the UAS results in a motion of the marker that does not contain rapid accelerations or continuous motion in a straight line.

2) The motion-capture system has tracking position accuracy on the order of 1 m throughout the capture volume without discontinuities in accuracy as a function of position within the volume.

3) Motion-capture position estimates contain error in the form of bias and noise, but these measurements can be filtered to remove noise and differentiated to estimate an accurate marker velocity over short segments of time. By differentiating the position measurements to estimate velocity, position bias error that is assumed constant over short distances does not influence the velocity estimate.

The algorithm to correct timing errors in the TS16 measurements uses the following approach:

1) Loop through short overlapping segments of TS16 data, using a segment length of 20 s.

2) Identify measurements collected by the motion-capture system that overlap this segment plus or minus a short buffer.

3) Filter the motion-capture position estimates by using a two-pass moving average filter to reduce measurement noise.

4) Bias the motion-capture estimate to the midpoint of the TS16 segment. This creates a reference signal equivalent to integrating the motion-capture

velocity forward and backward in time from the midpoint of the TS16 segment.

5) Shift the timestamps of each point of TS16 data in the segment to minimize horizontal position offset as a function of time between the individual point and the reference signal. A maximum time correction limit of ±0.3 s is enforced.

6) Shift the time bias of the entire segment to minimize average position offset between the segment and the raw motion-capture position data. This step addresses the timing error of the TS16 point at the segment midpoint since all other timestamps were corrected relative to this point.

7) Save the corrected time values for the middle 50% of the segment. Using overlapping segments in this manner serves two functions in this implementation:

   - Correcting only those timestamps within a short window on either side of the midpoint of the longer segment minimizes the effect of variable bias in the motion-capture data as a function of time.
   - Maintaining overall segment length adequate to ensure a curved portion of the UAS flight is captured minimizes the possibility of shifting the entire segment to obscure bias error in the motion-capture data parallel to the direction of travel of the UAS.

8) Establish corrected timestamps for the entire TS16 data set by assembling the corrected timestamps from each of the processed segments

The results of the algorithm described are shown in Fig. A-2 for a portion of the same time segment presented in Fig. A-1. Shown in black are TS16 position measurements as a function of time with corrected timestamps.

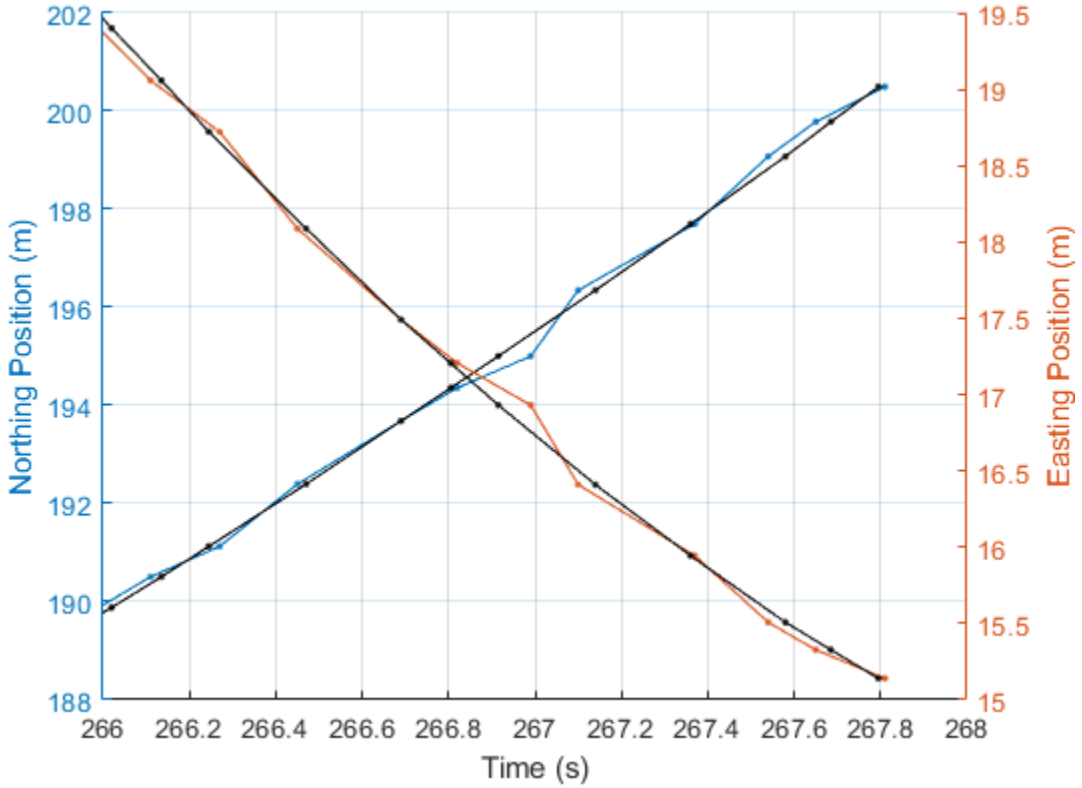

Fig. A-2 Comparison of raw TS16 position measurements and the same measurements with timestamp corrections applied (shown in black)

It is useful to examine the distribution of time correction applied to each point from the TS16 data to quantify the magnitude of the timing errors in the data. That distribution is shown in Fig. A-3.

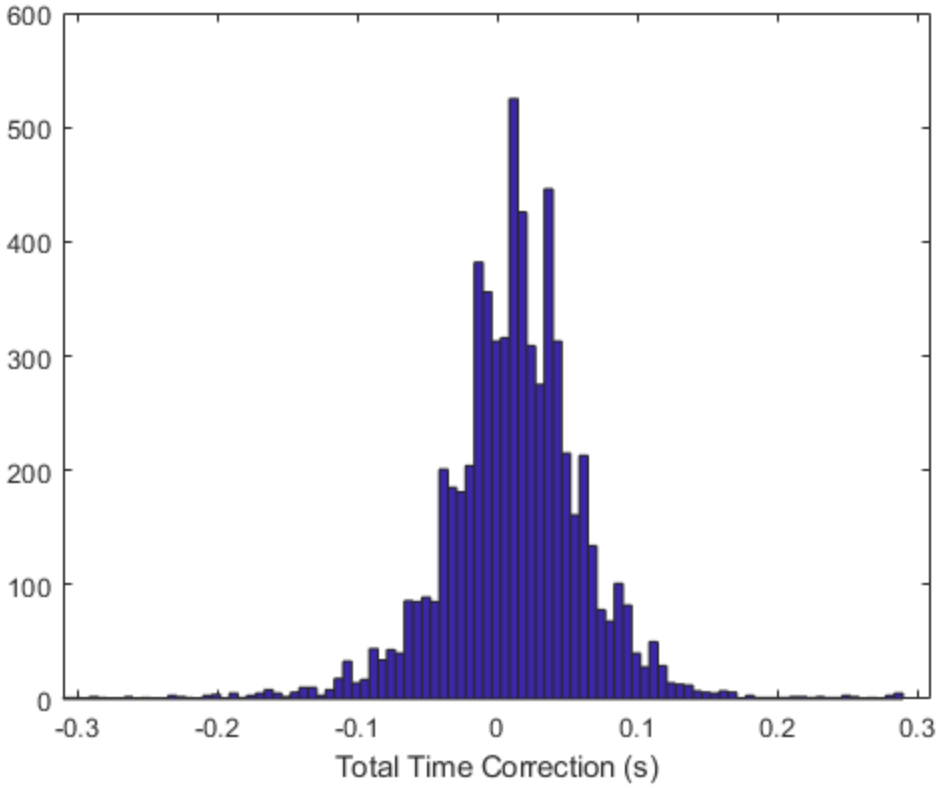

Fig. A-3 Distribution of time correction applied to individual TS16 position measurements

The effect of time in evaluating the accuracy of the collected motion-capture data can be visualized by examining the error vectors tracing individual measurements back to the ground-truth position used to calculate the error for that measurement. Visualizing the data in this manner makes it apparent that even though the motion-capture data exhibit a variable amount of position error in the direction parallel to the flight path of the UAS, the error rays trace back to the ground-truth signal incrementing steadily forward as would be expected. A representative example is shown in Fig. A-4.

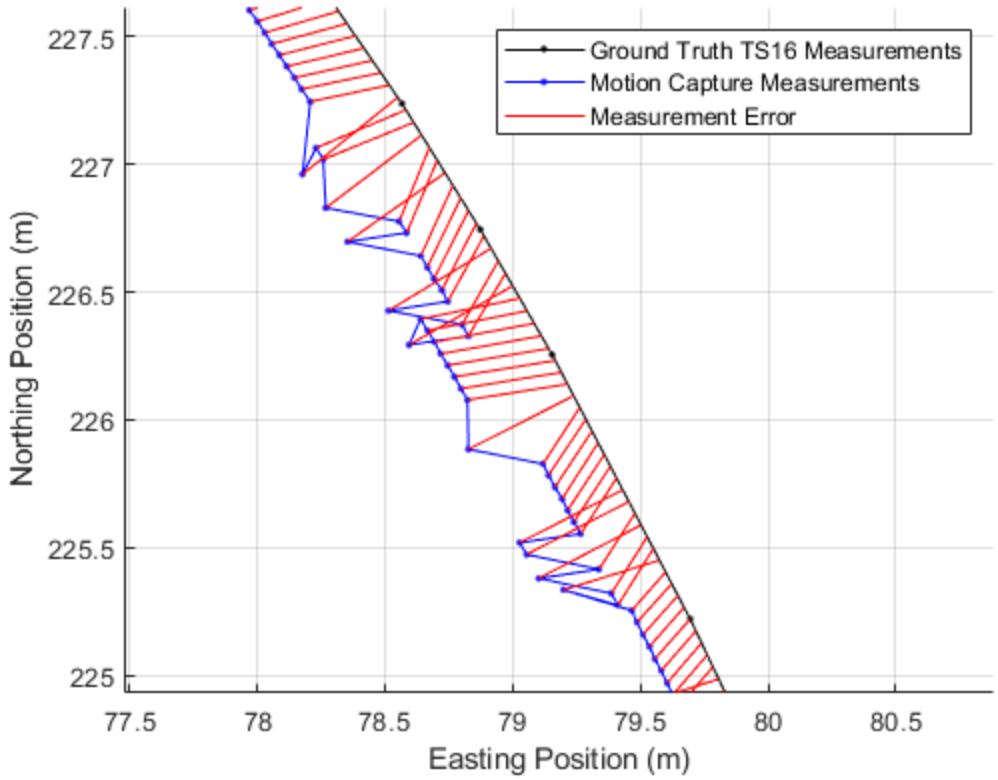

Fig. A-4 Representative example of position-error traces between motion-capture measurements and the ground-truth data implying the relationship between position and time for calculation of the position error

As discussed previously, it is important that the design of this algorithm be robust against biasing the timestamp corrections in such a way as to obscure error in the motion-capture system measurements. Three attributes of the implemented approach serve this purpose. First, only the timestamps of the TS16 data are adjusted. Measurement error in the motion-capture position measurements that is orthogonal to the direction of travel of the UAS is not affected by adjusting the TS16 timestamps. Second, only the filtered relative velocity estimated from the motion-capture system measurements is used as an input to correct individual TS16 timestamps. Bias error and measurement noise in the position measurements does not influence the point-by-point timestamp correction. Third, segments of adequate length are used to ensure curved portions of the flight path are represented when adjusting the time bias of the segment midpoint. This is the only step when absolute position measurements from the motion-capture system have the potential to skew the timestamp corrections to reduce the apparent measurement error of the motion-capture measurements compared with the ground truth. By using curved segments of the UAS flight path to determine the timing error of the segment

midpoint, any tendency of the algorithm to reduced apparent measurement error parallel to the direction of the UAS velocity is minimized.

While the TS16 timestamp correction algorithm has been specifically designed to reduce the possibility of skewing the ground truth toward the motion-capture measurements, there is inherently some minor reduction in the apparent motion-capture position-measurement error associated with this approach. It is believed that this effect is negligible compared with the accuracy of the TS16 instrument used as the source of ground-truth data. However, the position-measurement performance results presented in this report likely contain a slight underrepresentation of the true error due to the use of motion-capture measurements in correcting the TS16 timestamps.

List of Symbols, Abbreviations, and Acronyms

3-D	3-dimensional
AC	alternating current
ARL	Army Research Laboratory
ASCII	American Standard Code for Information Interchange
DOF	degrees of freedom
GPS	Global Positioning System
LED	light-emitting diode
PCB	printed circuit board
PCWDE	Precision and Cooperative Weapons in a Denied Environment
SEP	spherical error probable

1 (PDF)	DEFENSE TECHNICAL INFORMATION CTR DTIC OCA
1 (PDF)	CCDC ARL FCDD RLD CL TECH LIB
2 (PDF)	CCDC ARL FCDD RLW LF D EVERSON B KLINE